Dimensional analysis and calibration of a power model for compressive strength of solid-clay-brick masonry

Original
Dimensional analysis and calibration of a power model for compressive strength of solid-clay-brick masonry / Ferretti, D.. - In: ENGINEERING STRUCTURES. - ISSN 0141-0296. - 205:(2020), p. 110064. [10.1016/j.engstruct.2019.110064]

Availability:
This version is available at: 11381/2870648 since: 2021-01-04T18:18:36Z

Publisher:
Elsevier Ltd

Published
DOI:10.1016/j.engstruct.2019.110064

Pre-print
The published version of this manuscript is reported in:
Engineering Structures
Volume 205, 15 February 2020
DOI: 10.1016/j.engstruct.2019.110064

Dimensional analysis and calibration of a power model for compressive strength of solid-clay-brick masonry

Daniele Ferretti[a,*]

[a] *Department of Engineering and Architecture, University of Parma, Viale delle Scienze 181/A, I 43124 Parma, Italy*

Abstract

In the present work, the power model adopted to predict compressive strength of masonry as a function of brick and mortar strengths was studied by means of Dimensional Analysis, identifying the main dimensionless groups ruling the problem. The approach was applied on a dataset of solid-clay-brick masonry tests collected from the literature. Data were represented in a novel way that permitted to display the importance of the main dimensionless parameters. The dataset was filtered distinguishing these parameters and used to propose a new calibration of the power model considering mortar type and geometry of the specimens. Results show an interesting improvement in terms of indicators of regression quality with respect to the power models proposed in the literature. Both Dimensional Analysis and regressions confirm that the power models are specific for the type of specimens, i.e. dimensionless parameters, used for their calibration and direct comparisons among them should be done with great caution.

Keywords: A. Compressive strength, B. solid clay masonry, C. Eurocode 6, D. statistical analysis, E. dimensional analysis

---

1. Introduction

Forecasting masonry compressive strength as a function of geometrical and mechanical properties of its components is a challenging task that puzzled researchers since the beginning of twentieth century [1].

Usually, the compressive strength of masonry is determined as a function of brick and mortar strengths by means of: (a) tables [2] or phenomenological relationships [3, 4] calibrated by means of experimental data; (b) mechanical models based on linear/nonlinear behavior of mortar and bricks [5–8]; (c) nonlinear finite element models of wall specimens [9–13].

One of the most commonly adopted phenomenological relationship, which is frequently used as basis for comparison for new models, is the expression

$$f_M = K f_b^{\alpha} f_m^{\beta} \tag{1}$$

where f_M is the strength of masonry, f_b and f_m are the mean compressive strengths of bricks and mortars joints respectively, and K, α, and β are coefficients calibrated through the best fitting of a proper set of experimental data. Hereafter, subscripts M, b, and m stand for masonry, brick, and mortar respectively, while Eq. (1) will be called "power equation" because of the exponents, or powers, α, and β.

Several authors have calibrated the coefficients of the power equation by means of best fitting of experimental data with different types of bricks and blocks. A long list can be read in [14–16].

Although the method can be applied to any type of bricks, the present work concentrates on solid-clay-bricks, which are particularly common in existing masonry buildings, especially in monumental ones. Considering the related literature, it is mandatory to start from ENV1996-1-1 [17], briefly EC6, which provides an expression for the compressive strength of new masonry walls. For this reason, the power equation is also called "EC6-like" equation. The coefficient K varies between 0.4 and 0.7 depending on the brick types and construction details, such as thickness of bed joints, presence of head joints, and thickness of the wall. Furthermore, the formula is valid for $f_b < 75$ MPa, $f_m < 20$ MPa, and $f_m < 2f_b$ if the units are laid on general-purpose mortar. In case of multi-leaf walls, the strength is multiplied by the coefficient 0.8. Malek [18] and Hendry and Malek [19] analyzed full-scale story-height brickwork walls and observed that the coefficients are sensitive to the wall thickness (102.5 and 215 mm) and to the mortar type. Lumantarna et al. [20] calibrated the equation using both New Zealand historical field-extracted and laboratory-constructed three-brick high prisms composed of historical clay bricks and mortar. Mann [21] analyzed 925 specimens with bricks of different typologies (aerated concrete, lightweight concrete, sandstone, and solid clay). Kaushik et al. [22] fitted the results of 17 specimens (5 stacked bond bricks) in solid clay. Gumaste et al. [23] studied Indian stack-bonded prisms characterized by solid-clay-bricks that were relatively softer than mortar. Also Dayaratnam [24] studied specimens of Indian masonry.

Table 1 shows the coefficients proposed by the aforementioned authors. For EC6 [17] the values of solid clay units (group 1), general-purpose mortar, and single-wythe masonry have been written. For Hendry and Malek [19], the coefficients for walls with thickness $t_M = 102.5$ mm have been reported. All the expressions considered provide the mean compressive strength except EC6, which deals with the characteristic one.

In addition, Table 1 shows the values of the coefficient of determination R^2 declared by the authors, when available, which allows a concise judgment about the quality of the best fittings, i.e. a measure of the scatter between the values predicted by the formula and the experimental data. The closer the value of R^2 comes to 1, the better is the approximation.

The values of R^2 have not been published for all the considered cases and the confidence intervals of the coefficients are not available. Without these data, it is impossible comparing the accuracy of the formulae. Furthermore, it can be noticed that the coefficients proposed by the authors are quite different: K goes from 0.28 to 0.83 and α from 0.49 to 0.85. This is due to the inevitable statistical dispersion of the experimental results, as well as to the different types of specimens analyzed.

To compare the models proposed by the cited authors, the equations are plotted in Fig. 1 for mortar strengths f_m equal to 1.0 MPa and 10.0 MPa. As can be seen, the curves are quite dispersed. Small variations of the coefficients cause very different predictions. For instance, for a mortar strength $f_m = 1.0$ MPa and bricks with compressive strength $f_b = 15$ MPa, which are typical values for an historical masonry made with solid-clay-bricks and aerial lime mortar, the equations predict a masonry strength ranging from 1.0 to 5.7 MPa (Fig. 1a). The degree of uncertainty is very important. For the same masonry type, a table in the Italian code standard [2] recommends a value within the range of 2.6 to 4.3 MPa, regardless of mortar and brick strengths.

For more accurate predictions, the choice of a suitable formula is necessary. Aims of the present work are: (a) understand advantages and limits of the power models; (b) find which power model proposed in the literature is more suitable to forecast the strength of masonry built with solid-clay-bricks; (c) understand if the models proposed for general-purpose mortar are also valid in the case of lime mortar (which is particularly important for historical buildings but also for new ones made with lime mortar); (d) propose a new calibration specific for solid-clay-brick masonry considering also the mortar type; (e) discuss the quality of fitting and quantify the errors on the predicted strengths.

To this purpose, the structure of the power equation was here interpreted, probably for the first time, by means of Dimensional Analysis. The role of the different parameters affecting the compressive strength (e.g. the geometry of the specimens, the type of mortar, or the thickness of mortar joints) was discussed in terms of dimensionless groups. Then, a dataset gathered from the existing literature was collected and discussed considering these dimensionless groups. Subsequently, the dataset was clustered in order to obtain subsets with homogeneous values of the dimensionless groups and was used for a new calibration of the power model. Finally, the quality of the new best-fitted parameters was discussed considering their confidence intervals and three regression estimators.

Model	$\boldsymbol{K}$	$\boldsymbol{\alpha}$	$\boldsymbol{\beta}$	$\boldsymbol{R^2}$
Eurocode 6 [17]	0.55	0.70	0.30	–
Hendry and Malek [19]	1.29	0.52	0.19	
Lumantarna et al. [20]	0.75	0.75	0.31	0.87
Mann [21]	0.83	0.67	0.18	–
Kaushik et al. [22]	0.63	0.49	0.32	0.93
Gumaste et al. [23]	0.23	0.85	0.15	–
Dayaratnam [24]	0.28	0.50	0.50	–

Table 1: Power model $f_M = K f_b^{\alpha} f_m^{\beta}$ for masonry compressive strength: coefficients proposed by some authors and corresponding coefficient of determination R^2.

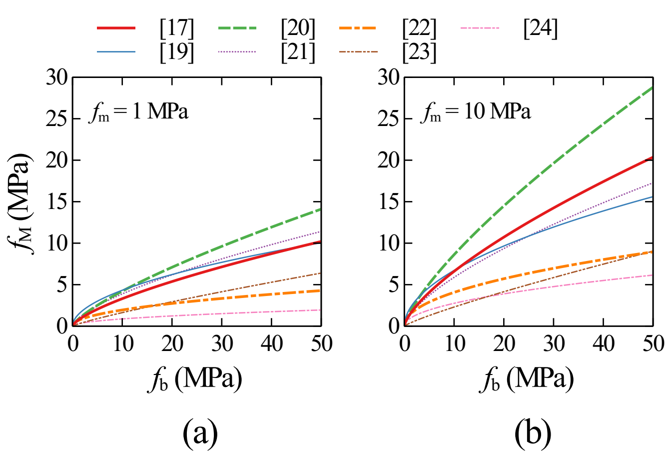

Fig. 1: Comparison of different power models proposed in the literature to evaluate the compressive strength of masonry f_M as a function of brick strength f_b: (a) mortar strength $f_m = 1$ MPa; (b) $f_m = 10$ MPa.

2. Dimensional analysis

2.1. Application of Dimensional Analysis to masonry compressive strength

Dimensional Analysis provides useful information when it is necessary to identify phenomenological equations whose structure is unknown [25–27]. The key stone of Dimensional Analysis is the Buckingham Π theorem, which states that given a functional relationship $g(.)$ between m dimensional variables (with physical dimensions) $q_1, q_2, \ldots, q_m$

$$q_1 = g(q_2, q_2, \ldots, q_m) \tag{2}$$

then it is possible to express the process as a function of $n = m - r$ dimensionless parameters $(\Pi_1, \Pi_2, \ldots, \Pi_{m-r})$ as

$$\Pi_1 = \tilde{g}(\Pi_2, \Pi_3, \ldots, \Pi_{m-r}) \tag{3}$$

where r is the number of m variables which are dimensionally independent (equivalent to the rank of the dimensional matrix).

To apply Buckingham theorem to the case of masonry compressive strength f_M, we start by expressing f_M as a function of all the parameters that have been recognized in the literature as the main factors governing the problem (a clear description is reported for instance in [28] and [29]):

$$f_M = g(\underbrace{f_b, f_{tb}, E_b, f_m, f_{tm}, E_m, \nu_b, \nu_m, f_{fb}, f_{vb}}_{\text{mechanical properties}}, \underbrace{h_b, b_b, t_b, h_M, b_M, t_M, h_m}_{\text{geometric properties}}, c_{sh}, \dot{\sigma}, \dot{\epsilon}), \tag{4}$$

where $f_b, f_{t,b}, E_b$ are compressive strength, tensile strength and Young modulus of bricks, $f_m, f_{t,m}, E_m$ are compressive strength, tensile strength, and Young modulus of mortar, ν_b, ν_m are Poisson coefficients of bricks and mortar respectively, f_{fb} and f_{vb} are the brick-mortar flexural and shear bond strengths respectively, h_b, b_b, t_b and h_M, b_M, t_M are height, length, and thickness of bricks and masonry specimens respectively, h_m is the height of mortar joints, c_{sh} is a shape factor which takes into account the type of brickwork bond, $\dot{\sigma}$ is the loading rate, and $\dot{\epsilon}$ is a strain rate similar to the one adopted in [30]. Eq. (4) describes the problem with $m = 18$ dimensional variables and three dimensionless parameters.

The mechanical problem can be defined in terms of three fundamental variables, e.g. mass M, length L, and time T. The corresponding dimensional matrix (of the dimensional variables) is:

$$\begin{array}{c|cccccccccccccccccc} & f_M & f_b & f_{tb} & E_b & f_m & f_{tm} & E_m & f_{fb} & f_{vb} & h_b & b_b & t_b & h_M & b_M & t_M & h_m & \dot{\sigma} & \dot{\epsilon} \\ \hline M & 1 & 1 & 1 & 1 & 1 & 1 & 1 & 1 & 1 & 0 & 0 & 0 & 0 & 0 & 0 & 0 & 1 & 0 \\ L & -1 & -1 & -1 & -1 & -1 & -1 & -1 & -1 & -1 & 1 & 1 & 1 & 1 & 1 & 1 & 1 & -1 & 0 \\ T & -2 & -2 & -2 & -2 & -2 & -2 & -2 & -2 & -2 & 0 & 0 & 0 & 0 & 0 & 0 & 0 & -3 & -1 \end{array} \tag{5}$$

The rank of the matrix is $r = 3$, therefore, according to the Buckingham theorem, the (maximum) number of dimensionless groups that rule the problem is $n = m - r = 15$. Following the Buckingham's theorem, the dimensionless strength Π_1 can be expressed as a function of 14 dimensionless groups $(\Pi_2, \dots, \Pi_{15})$ and 3 dimensionless parameters (ν_b, ν_m, c_{sh}) as:

$$\Pi_1 = \tilde{g}(\Pi_2, \Pi_3, \dots, \Pi_{15}, \nu_b, \nu_m, c_{sh}). \tag{6}$$

Buckingam's theorem provides the number of independent dimensionless groups Π but their form remains unknown. Furthermore, the choice of Π groups is not unique and identifying the most meaningful for a specific problem is not a trivial task.

2.2. Choice of the dimensionless groups

To define the dimensionless groups it is convenient to refer to groups usually recognized as important, bearing a physical meaning, in the literature on masonry. A possible expression is:

$$\frac{f_M}{f_b} = \tilde{g}\left(\frac{f_{tb}}{f_b}, \frac{E_b}{f_b}, \frac{f_m}{f_b}, \frac{f_{tm}}{f_b}, \frac{E_m}{f_b}, \frac{f_{fb}}{f_b}, \frac{f_{vb}}{f_b}, \frac{b_b}{h_b}, \frac{t_b}{h_b}, \frac{h_M}{h_b}, \frac{b_M}{h_b}, \frac{t_M}{h_b}, \frac{h_m}{h_b}, \frac{\dot{\sigma}}{\dot{\epsilon} f_b}, \nu_b, \nu_m, c_{sh}\right) \tag{7}$$

which is one of the simplest, but other groups are possible. For instance, the group h_M/h_b could be replaced with the group $(h_M/t_M) \times (t_M/t_b) \times (t_b/h_b)$ where the ratio (h_M/t_M) is called slenderness of the specimen and (t_M/t_b) is the number of wythes. Besides, in [28] the shape factor c_{sh} is replaced with the volume fraction of bricks VF_b (i.e., the ratio between volume of bricks and that of the specimen) and the volume fraction of mortar VR_{mH} (i.e., the ratio between volume of mortar in horizontal joints and total volume of mortar); both could be here considered as alternative dimensionless groups. Furthermore, if mortar is not applied uniformly, it is necessary to introduce the ratio of the bed-joint area to the gross area.

It is important to notice that not all the groups have the same relevance, and some choices could be better than others.

2.3. Reducing the number of dimensionless groups

It is still difficult to calibrate a phenomenological equation with all this dimensionless groups, because the number of variables is high. In general, it would be convenient to reduce the number of variables and consequently the enormous number of tests that need to be performed to calibrate the equation.

This is possible, for instance, considering that the tensile strength f_{tb} and the Young modulus E_b of the bricks are dependent variables since they can be written as a function of the compressive strength f_b by means of empirical equations like $f_{tb} = c_1 f_b^{c_2}$ and $E_b = c_3 f_b^{c_4}$, where c_1, c_2, c_3, c_4 are suitable coefficients [31]. In this case, the variables $f_{t,b}/f_b$ and E_b/f_b can be removed from Eq. (7) introducing an uncertainty related to the adopted empirical equations. The same simplification can be done for the mortar, so obtaining

$$\frac{f_M}{f_b} = \tilde{g}\left(\frac{f_m}{f_b}, \frac{f_{fb}}{f_b}, \frac{f_{vb}}{f_b}, \frac{b_b}{h_b}, \frac{t_b}{h_b}, \frac{h_M}{h_b}, \frac{b_M}{h_b}, \frac{t_M}{h_b}, \frac{h_m}{h_b}, \frac{\dot{\sigma}}{\dot{\epsilon} f_b}, \nu_b, \nu_m, c_{sh}\right) \tag{8}$$

and reducing to $m = 11$ the number of dimensionless variables, plus three parameters. However, we notice that the coefficients c_i of the adopted empirical expressions change with the type of brick and mortar, and therefore Eq. (8)

should refer in principle to a specific type of brick (e.g. extruded clay, pressed clay, calcium silicate, concrete, etc.) and mortar (e.g. cement, cement-lime, or lime). In other words, while Eq. 7 is quite general allowing a unified approach to the problem, Eq. 8 is specific, at least in principle, for a certain type of units and binder because it does not explicitly consider their different mechanical properties.

Further simplifications derive from the evidence that, in many tests, some variables assume a constant value. To the purpose, Sonin [32] demonstrated that, given a functional relationship between m quantities, of which r are dimensionally independent, if m_k quantities assume constant value in all the cases being considered, then it is possible to express the process as a function of $n = m - r - (m_k - r_k)$ dimensionless groups, where r_k is the number of m_k variables which are independent (equivalent to the rank of the dimensional matrix) [32]. In passing, this is not equivalent to eliminate the role of the constant dimensionless groups in describing the process, but simply gives the possibility to neglect those constant groups in the interpretation of the experiments.

Following Sonin's theorem, one might perform the tests by using bricks of standard (constant) dimensions. In this case, h_b, b_b, and t_b are constant and their corresponding dimensional matrix (in terms of dimensional variables)

$$\begin{array}{c|ccc} & h_b & b_b & t_b \\ \hline M & 0 & 0 & 0 \\ L & 1 & 1 & 1 \\ T & 0 & 0 & 0 \end{array} \tag{9}$$

involves $m_k = 3$ variables whereas the rank of this matrix is $r_k = 2$. The dimensional matrix in Eq. 9 is a sub-matrix of the one in Eq. 5. Applying Sonin's theorem, the number of dimensionless groups becomes $n = m - r - (m_k - r_k) = 9$. In other words, performing the tests by using standard-size bricks would simplify data interpretation permitting, for instance, to remove the dimensionless groups b_b/h_b and t_b/h_b from Eq. (8), obtaining:

$$\frac{f_M}{f_b} = \tilde{g}\left(\frac{f_m}{f_b}, \frac{f_{fb}}{f_b}, \frac{f_{vb}}{f_b}, \frac{h_M}{h_b}, \frac{b_M}{h_b}, \frac{t_M}{h_b}, \frac{h_m}{h_b}, \frac{\dot{\sigma}}{\dot{\epsilon} f_b}, \nu_b, \nu_m, c_{sh}\right) \tag{10}$$

Of course, this simplification absolutely does not mean that the size of the bricks is physically irrelevant; it is just an experimental assumption that permits to focus on the effect of the other dimensionless parameters.

2.4. Dimensional analysis and power equation

Dimensional Analysis does not provide information on the analytical expression for the equation $\tilde{g}(.)$ governing the problem.

The analytical expression of $\tilde{g}(.)$ can be chosen to be particularly suitable for data fitting and regression algorithms. This is the case of the equation:

$$\frac{f_M}{f_b} = k\left(\frac{f_m}{f_b}\right)^{\beta_1} \times \left(\frac{f_{fb}}{f_b}\right)^{\beta_2} \times \left(\frac{f_{vb}}{f_b}\right)^{\beta_3} \times \left(\frac{b_b}{h_b}\right)^{\beta_4} \times \left(\frac{t_b}{h_b}\right)^{\beta_5} \times \ldots \tag{11}$$

where $k, \beta_1, \beta_2, \ldots$ are coefficients. The equation is obtained by multiplying the powers of all the dimensionless groups in Eq. (8). If only the dimensionless group f_m/f_b varies whereas all the other remain constant, Eq. (11) becomes:

$$\frac{f_M}{f_b} = K\left(\frac{f_m}{f_b}\right)^{\beta} \tag{12}$$

or

$$f_M = K f_b^{1-\beta} f_m^{\beta} = K f_b^{\alpha} f_m^{\beta} \tag{13}$$

with $\alpha = 1 - \beta$, which is the well-known power equation usually adopted in the literature for masonry compressive strength (Eq. 1).

Equation (13), like Eq. (8), is specific for a given type of unit and binder because it does not explicitly consider their different mechanical properties. It is evident from Eq. (12) that, if just one of the constant dimensionless groups not explicitly considered in Eq. (13) varies, the coefficients of the equation will be different. This clearly explains the important differences between dimensionless coefficient K of the power equations proposed in the literature (Tab. 1). The variations of the exponents α and β can be explained considering that

Eq. (12) is oversimplified; for instance also the powers β_i could be functions of the dimensionless parameters.

From a mechanical viewpoint, these differences can be explained considering that masonry specimens display different failure modes depending both on the properties of brick and mortar and on the loss of bond between them [33]. In [23] four different failure modes were observed: in case of bricks stiffer than mortar, a triaxial compression occurs in the mortar whereas bricks are subjected to compression/biaxial tension up to possible debonding between the two materials. In case of mortar stiffer than bricks, instead, the triaxial compression occurs in the bricks whereas mortar is subjected to compression/biaxial tension. Assuming that there is a relationship between stiffness of the components and their compressive strength, it is possible to suppose that the behavior is ruled by the ratio f_m/f_b. This scenario is modified by the presence of vertical mortar joints (considered by coefficient c_{sh}) and by loss of bond between bricks and mortar (accounted by f_{vb}/f_b and f_{fb}/f_b). The structure of Eq. (13) is too simple to catch all failure modes and distinct procedures of calibration and coefficients are necessary, at least for the two cases of bricks stronger and weaker than mortar (i.e. $f_m/f_b > 1$).

The use of the Dimensional Analysis has proven some theoretical limits of the power equation and has explained the variability of its coefficients. In the next section these aspects will be considered for a proper calibration of a new power equation.

3. Experimental dataset

3.1. Description of the dataset

In order to discuss the power equation, it was necessary to collect a database of experimental data that comprehends all the dimensionless variables grouped in Eq. (8). Because the equation is specific to a given type of brick and mortar, it was necessary to limit the attention to a certain type of masonry. For the reasons explained in the introduction, the database has been prepared by

	$\boldsymbol{f}_M$ (MPa)	$\boldsymbol{f}_b$ (MPa)	$\boldsymbol{f}_m$ (MPa)	$\boldsymbol{b}_b$ (mm)	$\boldsymbol{t}_b$ (mm)	$\boldsymbol{h}_b$ (mm)	$\boldsymbol{h}_M$ (mm)	$\boldsymbol{t}_M$ (mm)	$\boldsymbol{h}_m$ (mm)
min	0.74	6.81	0.60	200.0	100.0	50.0	300.0	100.0	8.00
mean	7.84	17.68	5.74	239.4	115.3	59.7	441.8	151.2	10.55
max	14.98	32.00	13.85	280.0	140.0	75.5	800.0	260.0	15.00

Table 2: Variations of the parameters of the analyzed dataset for wallettes.

searching the literature for compression tests on specimens made of solid-clay-bricks. Of course, the approach that will be followed, being completely general, is also valid for other types of masonry, such as concrete block masonry. Only wallettes and stack-bonded prisms specimens were considered because they received more attention in the literature. To collect the data, the database MADA [34] has also been used. Unfortunately, many studies with interesting experimental campaigns have been discarded because they contained incomplete data. Specimens with bricks weaker than mortar have been discarded too, since they display a different failure mode with respect to the one with bricks stronger than mortar [35], which are the majority of experimental data. Finally, a set of 116 values from 24 references has been collected [6, 18, 20, 23, 36–55]. The data are reported in Tabs. A1 and A2 of the Appendix, for wallettes and stack-bonded prism specimens respectively. The tables include the strengths of masonry f_M, bricks f_b, and mortar f_m, the dimensions of both walls ($b_M \times h_M \times t_M$) and bricks ($b_b \times h_b \times t_b$), and the thickness of mortar joints h_m. In addition, available information on number of wythes, and mortar type (cement c, cement-lime $c + l$, and lime l) have been indicated. Bond strengths f_{fb} and f_{vb} were not reported because of the scant or null information in the considered experimental campaigns.

Wallettes and stack-bonded prisms display a different behavior [56], therefore they have been studied separately taking into account implicitly the shape parameter c_{sh}. According to EC6 [17], tests on wallettes are performed following EN1052-1 [57] code, which prescribes standard values for the load speed. For this reason, the dimensionless parameter $\dot{\sigma}/\dot{\epsilon} f_b$ can be considered constant.

	$\boldsymbol{f}_M$ (MPa)	$\boldsymbol{f}_b$ (MPa)	$\boldsymbol{f}_m$ (MPa)	$\boldsymbol{b}_b$ (mm)	$\boldsymbol{t}_b$ (mm)	$\boldsymbol{h}_b$ (mm)	$\boldsymbol{h}_M$ (mm)	$\boldsymbol{t}_M$ (mm)	$\boldsymbol{h}_m$ (mm)
min	2.90	7.50	0.69	191.0	89.0	50.0	250.0	89.0	7.50
mean	13.33	29.22	9.33	229.6	109.2	62.3	313.8	109.7	12.13
max	37.70	68.73	52.60	290.0	140.0	78.0	523.0	140.0	15.00

Table 3: Variations of the parameters of the analyzed dataset for stack-bonded prisms.

	$\boldsymbol{f}_M/\boldsymbol{f}_b$ (–)	$\boldsymbol{f}_m/\boldsymbol{f}_b$ (–)	$\boldsymbol{b}_b/\boldsymbol{h}_b$ (–)	$\boldsymbol{t}_b/\boldsymbol{h}_b$ (–)	$\boldsymbol{h}_M/\boldsymbol{h}_b$ (–)	$\boldsymbol{h}_M/\boldsymbol{t}_M$ (–)	$\boldsymbol{t}_M/\boldsymbol{h}_b$ (–)	$\boldsymbol{h}_m/\boldsymbol{h}_b$ (–)
min	0.06	0.05	2.86	1.43	5.45	2.14	1.52	0.14
mean	0.45	0.33	4.11	1.99	7.63	3.11	2.69	0.17
max	0.86	0.83	5.09	2.55	11.80	4.17	5.20	0.21

Table 4: Variations of the dimensionless parameters of the analyzed dataset for wallettes.

	$\boldsymbol{f}_M/\boldsymbol{f}_b$ (–)	$\boldsymbol{f}_m/\boldsymbol{f}_b$ (–)	$\boldsymbol{b}_b/\boldsymbol{h}_b$ (–)	$\boldsymbol{t}_b/\boldsymbol{h}_b$ (–)	$\boldsymbol{h}_M/\boldsymbol{h}_b$ (–)	$\boldsymbol{h}_M/\boldsymbol{t}_M$ (–)	$\boldsymbol{t}_M/\boldsymbol{h}_b$ (–)	$\boldsymbol{h}_m/\boldsymbol{h}_b$ (–)
min	0.20	0.05	2.92	1.44	3.21	1.89	1.44	0.13
mean	0.53	0.35	3.84	1.82	5.20	2.92	1.83	0.20
max	1.08	1.00	5.80	2.80	8.77	5.51	2.80	0.30

Table 5: Variations of the dimensionless parameters of the analyzed dataset for stack-bonded prisms.

The same applies for stack-bonded prisms, which are usually tested according to ASTM 1314-18 [58]. Tables 2 and 3 show the minimum, mean, and maximum values of the parameters of wallettes and stack-bonded prisms datasets respectively. For the same datasets, Tables 4 and 5 represents the minimum, mean, and maximum values of the considered dimensionless parameters, already defined in Eq. (8). Tabs. 2, 4 show that wallettes substantially fulfill the mechanical and geometrical limits prescribed by EC6 [17] and EN1052-1 [57]. Also for stack-bonded prisms, Tabs. 3 and 5 show that the prescription of ASTM 1314-18 [58] are mostly satisfied.

The number of samples (41 and 75 for wallettes and stack-bonded prisms respectively), although limited, is sufficient to perform some statistical studies. However, since data have been measured sometimes with heterogeneous specimens and testing conditions, data preparation and discussion by means of Dimensional Analysis will be performed before proceeding with their study.

3.2. Correction of brick and mortar strengths

The power model employs the mean compressive strengths of bricks and mortar as input variables. For the considered dataset, these values have been measured following different standard codes, humidity conditions, and geometry of the specimens. Regarding the geometry, it is known that size and shape of brick specimens influence their failure mode and, consequently, the measured strength [59]. For this reason, EC6 [17] employs in the power equation the normalized strength $f_b' = \delta f_b$, where the coefficient δ, defined in EN772-1 [60], transforms the measured strength to the one of a reference cube of side 100 mm. The same correction coefficient δ was used in [61, 62] to homogenize their database of hollow concrete blocks. Since this correction seems to be accepted by the scientific community, it was used in the present work to compute the normalized brick strengths f_b' reported in Tabs. A1,A2.

Apart these tables, in the forthcoming sections the corrected brick strength f_b' will always be used although, for simplicity, it will be indicated as f_b.

Also the size and the slenderness of mortar samples have a recognized influence on the measured value of compressive strength f_m [63]. Unfortunately, many authors do not report the adopted standards, nor the size of the mortar specimens; therefore it was not possible to correct the values of f_m.

3.3. Correction for masonry slenderness

The slenderness of the specimens (i.e. the ratio of the height to the least lateral dimension of the prism h_M/t_M) plays an important role in masonry compressive strength [64–68]. The slenderness h_M/t_b should be chosen to correctly represent the behavior of real walls subjected to pure compression. For this reason, the slenderness should be limited to reduce the eccentricity due to construction imperfections and second order effects [68]. Furthermore, squat specimens are easier to build or extract from existing masonry and for this reason are allowed by different standard codes. In this case, a minimum of three courses of bricks ($h_M/h_b \geq 3$) is indispensable to prevent the effect of end restraints - exerted by the platens of the testing machine on the lateral deformation of the specimen - from altering the masonry failure mode [69]. As observed in [65], it seems that only for a slenderness $h_M/t_M > 6$, the effect of end restrains vanishes and pure compressive strength is attained. The restraints can be reduced by introducing a layer of suitable frictionless material between the specimen and the load bearing platens of the testing machine. Of course, different frictionless materials produce different effects on the measured strength [46, 55]. For this reason, some standard codes, rather than adopting frictionless interlayers, prefer to recommend a specific slenderness. For instance, Fig. 2 shows the sizes required by EN1052-1 [57] (for units with $h_b \leq 150$ mm and $b_b \leq 300$ mm) and ASTM 1314-18 [58] standard codes. Furthermore, the ASTM 1314-18 [58] adopts correction factors to transform the measured strength to the one of a reference specimen with slenderness $h_M/t_M = 2$. On the contrary, UNI 1052-1 [57] prescribes specimens with $h_M/t_M > 3$, without any correction factor.

The choice of a well-suited correction function is not trivial. The high number of solutions proposed in the literature as well as in standard codes reveals that the problem is still open [70]. For instance, in [61, 62] the ASTM 1314-18 correction function was used for concrete masonry prisms. In [28], instead, it was preferred to calibrate the correction function together with the power equation.

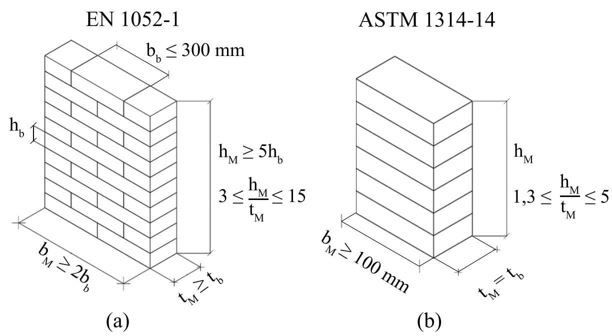

Fig. 2: Shape of masonry prisms recommended by Standard Codes: (a) EN1052-1 [57]; (b) ASTM 1314-18 [58].

In the present work, wallettes fulfill the geometric limits prescribed by EN1052-1 therefore, according to the same code, no correction function was introduced. On the contrary, test on stack-bonded prisms were performed according to ASTM 1314-18 and the correction function prescribed by the same code, which seems to be well accepted by the scientific community, was applied. The corrected compressive strengths f'_M thus obtained are reported in Tab. A2. Apart this table, in the forthcoming sections the corrected masonry strength f'_M will always be used for stack-bonded prisms but, for homogeneity with wallettes, it will be indicated as f_M.

3.4. Discussion of the dataset considering the dimensionless parameters

The corrected dataset is now discussed starting from wallettes. Fig. 3 shows the masonry dimensionless strength f_M/f_b as a function of mortar dimensionless strength f_m/f_b. In Fig. 3a the data are represented distinguishing the number of wythes (t_M/t_b). The figure clearly shows that two-wythes wallettes present smaller strengths with respect to one-wythe, as already highlighted by some authors [17, 19]. For this reason one-wythe and two-wythe data must be studied separately. In the collected dataset, one-wythe wallettes are the majority therefore the subsequent figures are specific for one-wythe masonry ($t_M/t_b = 1$). In Fig. 3b the data are represented considering the type of mortar (cement, cement-lime, and lime): differences between the three types are not so evident but deserve to be investigated. Fig. 3c represents the effect of the dimensionless parameter h_M/h_b, related to the number of courses, which is not self-evident. The same can be said for the slenderness h_M/t_M considered in Fig. 3d. This seems to justify, for the considered dataset, the choice of having omitted a correction factor for the slenderness. The effect of the thickness of mortar joints is represented in Fig. 3e by means of the dimensionless parameter h_m/h_b. Also in this case, data do not show different trends for the different values of h_m/h_b. Finally, Figs. 3f,g represent the effect of brick geometry by means of the dimensionless parameters t_b/h_b and b_b/h_b. Data display an homogeneous behavior; therefore the dimensionless sizes of the bricks can be considered to be constant, as in the previous example on Sonin's theorem. Based on this analysis, it seems correct to perform the best fitting of the dataset of wallettes by distinguishing the number of wythes and the type of mortar, whereas all the other dimensionless groups will be considered to be constant.

Considering stack-bonded prisms, Fig. 4a shows the importance of mortar type: imagining an ideal bisector line from the lower left to the upper right corners of the figure, points corresponding to lime mortar are clustered in the upper part with respect to this line. The effect of dimensionless parameter h_M/h_b can be observed in Fig. 4b. The most surprising aspect is that specimens with $6 < h_M/h_b \leq 8$ are clustered in the lower part of the plot whereas specimens with $2 < h_M/h_b \leq 4$ are grouped at the top. This effect is more evident in Fig. 4c where the slenderness h_M/t_M is considered: squat specimens are placed in the upper part of the plot whereas slender specimens are placed in the bottom part. The effect is evident also in case of uncorrected masonry strengths f_M (Figs. 4d). Interestingly, it seems that the adopted ASTM1314-18 correction function is not able to remove completely the effect of slenderness for

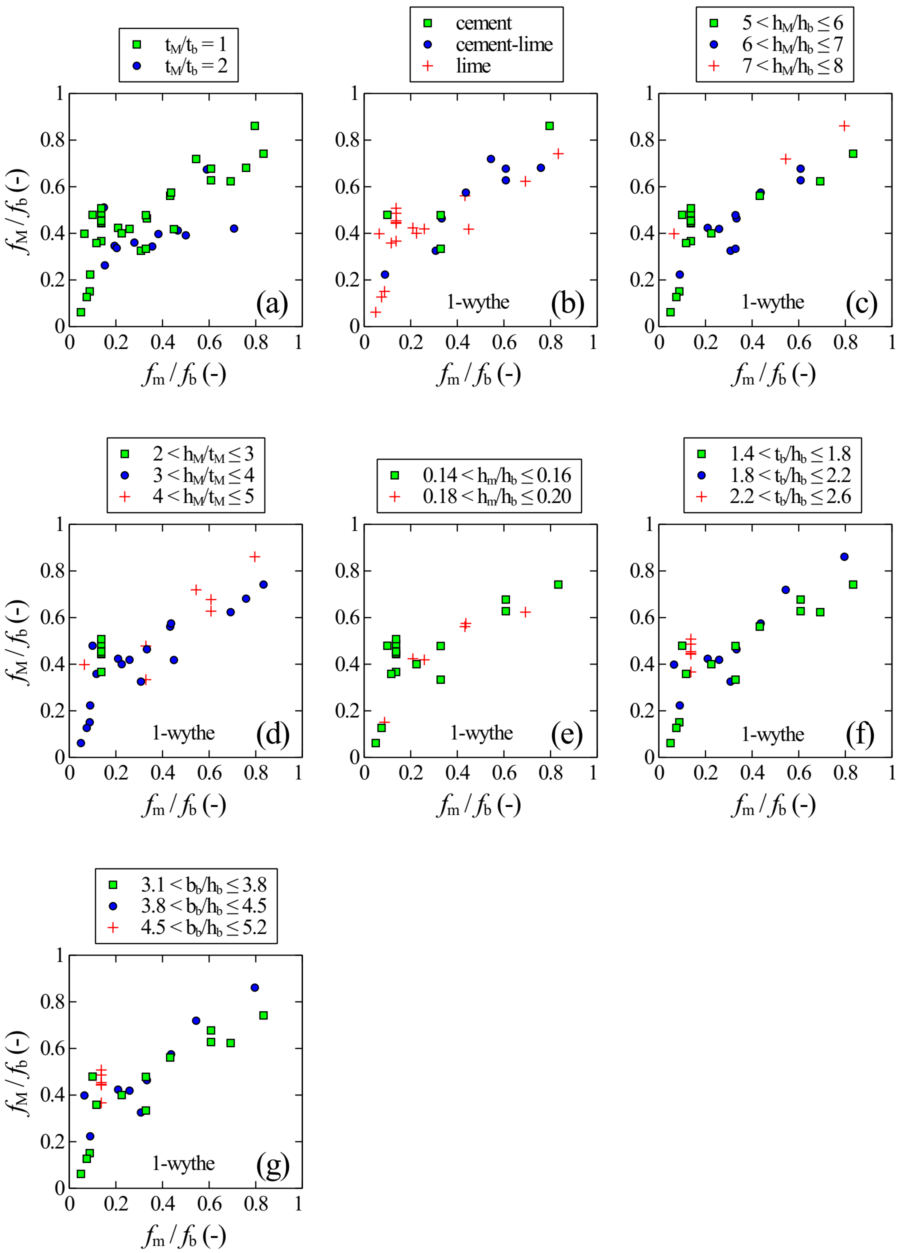

Fig. 3: Wallettes: (a) effect of the number of wythes t_M/t_b; (b) effect of mortar type; (c) effect of h_M/h_b; (d) effect of h_M/t_M; (e) effect of mortar joint thickness h_m/h_b; (f) effect of brick size t_b/h_b; (g) effect of brick size b_b/h_b.

the considered dataset. This problem has already been raised in [71] for concrete masonry prisms. Fig. 4e shows the effect of mortar thickness h_m/h_b. As in the case of wallettes, data do not display a specific trend. The same can be said for the brick dimensions t_b/h_b and b_b/h_b shown in Figs. 4f,g. According to this graphic analysis, it seems possible to perform the best fitting of the dataset of stack-bonded prisms by distinguishing the type of mortar and the slenderness of the specimens h_M/t_M, which seems to be the most meaningful dimensionless groups, whereas all the others will be considered to be constant.

4. Calibration of a new power equation

The obtained results suggest trying a new calibration of the power model – which is specific for solid clay bricks – by distinguishing the different dimensionless groups that have been recognized to be important for the collected dataset.

Generally, the coefficients of the power models proposed in the literature are calibrated by minimizing the sum-of-squares (SS) of the residuals $X = f_{M,test} - f_{M,model}$, defined as "vertical" distance between experimental points and surface, by means of the Minimum Least Square Method (MLSM). This method is based on the hypothesis that the residuals X follow a Gaussian distribution with constant variance (homoscedasticity). In addition, the method requires that independent variables are measured with much greater precision than the dependent ones. These hypotheses, which are usually taken for granted, are now verified before proceeding with the calibration of the model.

Here, the power equation

$$f_M = K f_b^{\alpha} f_m^{1-\alpha} \tag{14}$$

was used, where K and α are the parameters to be fitted. Equation (14) was preferred to Eq. (1) because it is more consistent from the point of view of dimensional analysis, since the coefficient K is dimensionless and does not change with the adopted units. Furthermore, Eq. (12) was not used because, when dividing f_M by f_b, the nonlinear transformation modifies also the distribution of

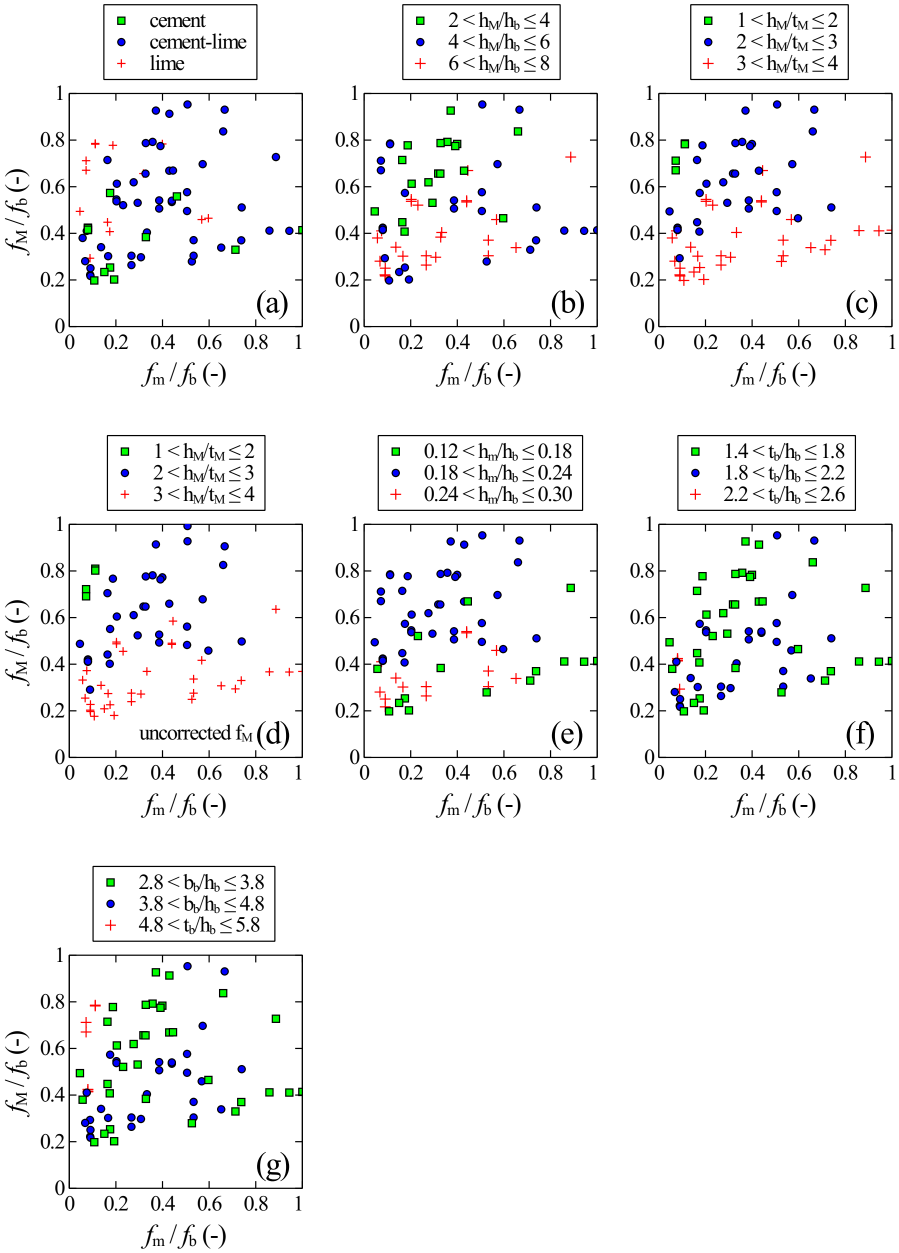

Fig. 4: Stack-bonded prisms: (a) effect of mortar type; (b) effect of h_M/h_b; (c) effect of slenderness h_M/t_M; (d) effect of slenderness h_M/t_M for uncorrected strengths f_M; (e) effect of mortar joint thickness h_m/h_b; (f) effect of brick size t_b/h_b; (g) effect of brick size b_b/h_b.

the residuals $|X|$, which, as we will see, has a certain importance for the study of the regression.

The employed equation requires to solve a problem of nonlinear regression with unknowns K and α. Transformation of Eq. (14) by means of logarithms would simplify the problem to a linear regression

$$\ln f_M = \ln K + \alpha \ln f_b + (1-\alpha) \ln f_m \tag{15}$$

with unknowns $\ln K$ and α. However, this transformation would also modify the distribution of the residuals X, and therefore it was not applied at this stage, where it was preferred to solve the nonlinear problem by using the Matlab function `fit` [72].

The fitting was initially performed considering 1-wythe wallettes. The best-fitting function is represented in Fig. 5a as a surface, together with the data points. The dispersion of the points is evident; however the analysis of the data by means of matlab FSDATool [73] reveals that this dispersion is not due to outliers, therefore robust statistics was not applied.

The values of the fitted parameters K and α, and their 95% confidence intervals, computed by means of the asymptotic method [72], are reported in Tab. 6 (wallettes 1-wythe). The 95% confidence interval has a 95% chance of containing the true value of the parameter. The corresponding upper and lower bound surfaces, plotted in Fig. 5a, show the uncertainty of the model.

The analysis of the residuals X permits to check if the adopted procedure fulfills the hypotheses of the MLSM. Fig. 5b shows the plot of the residuals X, together with their best fitting plane of equation $X = p_0 + p_1 f_b + p_2 f_m$. Small values of the coefficients p_0, p_1, and p_2 confirm that the errors X are equally distributed above and below the plane $X = 0$. Fig. 5c displays the absolute value of the error $|X|$ and the corresponding best-fitting plane. It is possible to observe that the errors, as expected, increase with f_b but the coefficients of the best fitting plane are small also in this case, therefore the hypothesis of constant variance (homoscedasticity) is not badly violated.

To check the hypothesis of normal distribution of the residuals X, their

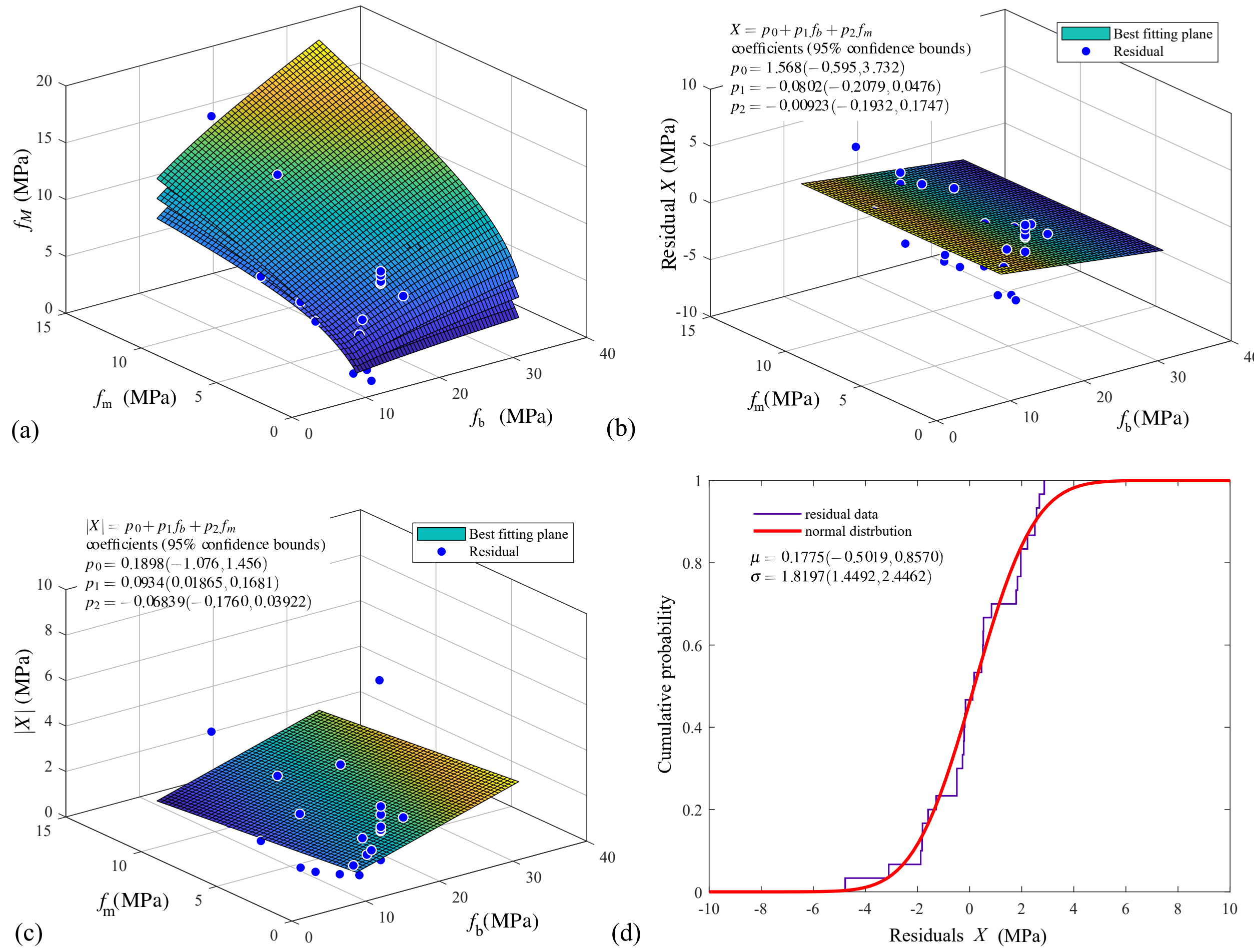

Fig. 5: Best fitting of all the data: (a) Comparison between best fitted model, 95% confidence bounds and experimental points; (b) Comparison between residuals X and their best-fitting plane; (c) Comparison between absolute values of the residuals $|X|$ and their best-fitting plane; (d) Cumulative of the residuals X and fitting with normal-distribution cumulative.

cumulative has been plotted in Fig. 5d. The theoretical normal cumulative, with mean $\mu = 0.1775$ MPa and standard deviation $\sigma = 1.8197$ MPa, is well superimposed on the experimental curve. In addition, normality tests have been performed. In particular, the skewness is -0.58 and Kurtosis coefficient

Type	**Param.**	**all**	**cement**	**cement-lime**	**lime**
Wallettes (1 wythe)	N	30	4	8	18
	K	0.79 (0.66, 0.91)	-	0.91 (0.66, 1.15)	0.70 (0.51, 0.89)
	α	0.57 (0.44, 0.70)	-	0.33 (0.022, 0.64)	0.70 (0.54, 0.86)
Stack-bonded prisms	N	35	5	22	8
$2 \leq h_M/t_M < 3$	K	0.87 (0.74, 1.01)	-	0.76 (0.50, 1.02)	0.75 (0.28, 1.21)
	α	0.71 (0.63, 0.80)	-	0.90 (0.55, 1.24)	0.74 (0.36, 1.11)
Stack-bonded prisms	N	33	6	24	1
$3 \leq h_M/t_M < 4$	K	0.57 (0.46, 0.68)	-	0.60 (0.47, 0.74)	-
	α	0.75 (0.61, 0.90)	-	0.73 (0.57, 0.90)	-

Table 6: Parameters of the model $f_M = K f_b^{\alpha} f_m^{1-\alpha}$ obtained by best fitting of N specimens, 95% confidence intervals (within parentheses).

is equal to 3.22. For a normal distribution, the skewness (which measures the lack of symmetry of the distribution) is zero and the Kurtosis coefficient (which measures how the data are tailed with respect to a normal distribution) is 3. With these values, it is possible to confirm the hypothesis of normal distribution of the residuals X.

The previous analyses of the errors show that the hypotheses of MLSM are substantially fulfilled. The only problem is that the independent variables (brick and mortar strengths) are measured with a precision comparable with the dependent ones, as suggested by their typical coefficients of variation. The problem is pointed out also in the EC6 [17], where it is specified that the proposed power equation is valid only for bricks whose compressive strength has a coefficient of variation smaller than 25%. To address this issue it would be necessary to develop new statistical tools based for instance on Total Least Squares Method [74–76], which are very complicate and out of the scope of the present work.

Considering the fact that all power models proposed in the literature ignored this issue obtaining satisfactory results, or at least accepted by the scientific community, MLSM was considered applicable to the problem also in the present work.

Therefore, fitting and validation were repeated to the sub-cases of 1-wythe wallettes in cement-lime, and lime mortar. The case of cement was not analyzed because of the insufficient number of experimental data ($N = 4$). The values of the determined coefficients K and α are reported in Tab. 6, together with their 95% confidence intervals.

The importance of confidence intervals is shown in Fig. 6, where the dimensionless masonry strength f_M/f_b is represented as a function of dimensionless mortar strength f_m/f_b. In the same figure, the fitted curve is represented together with the 95% confidence band obtained using the confidence intervals as coefficients of the power model. The confidence band shows how well we know the curve. The dispersion of the data and their limited number implies rather wide confidence bands. Probably the results would improve increasing the number of data points.

Fitting was repeated for stack-bonded prisms distinguishing slenderness $2 \leq h_M/t_M < 3$ and $3 \leq h_M/t_M < 4$. Results are reported in Tab. 6 considering all the data and, subsequently, separating the mortar type. Cases with $N < 8$ were not analyzed because of the scant number of points.

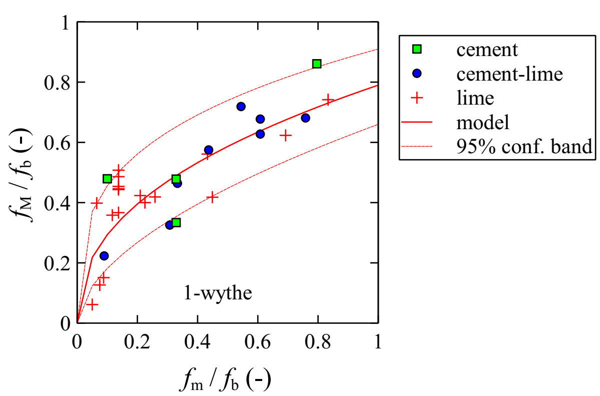

Fig. 6: Results of fitting of 1-wythe wallettes (all data) and corresponding confidence band.

Also in the case of stack-bonded prisms, coefficients reported in Tab. 6 display an important variation an wide 95% confidence limits.

Despite this problem, it is interesting to notice that the coefficients for stack-bonded prisms are different from the ones for wallettes. Furthermore, the different slenderness and mortar type imply, as expected, different coefficients.

5. Discussion of the results

5.1. Wallettes

The quality of the proposed regressions was investigated starting from one-wythe wallettes (all data). The predicted strengths $f_{M,model}$ are plotted in Fig. 7a as a function of the corresponding measured strengths $f_{M,test}$, together with the bisector line that represents the ideal perfect correspondence between the test results and the proposed model. Points above the bisector line lay on the unsafe side. In the same figure, the dashed lines represent an error of $\pm 20\%$ in the model.

The study is repeated in Fig. 7b for EC6 [17] model. A coefficient of 1.2 was used according to [17] to transform the characteristic strengths into the mean strengths. As can be seen, the results are similar to the ones of the proposed regression in the case of low strengths but some points lay on the unsafe side for higher strengths. Fig. 7c shows the behavior of the model proposed by Hendry & Malek [19]. In this case, most of the points lay on the safe side with important errors. The same can be said for the Mann's model [21].

To quantify numerically the goodness of the fit, the classic coefficient of determination R^2 was computed. Results are reported in Tab. 7. The proposed model provides the best R^2, especially when the type of mortar is distinguished. The values are not exciting, but in any case better than those of the models chosen for comparison, especially for cement-lime and lime mortar. However, it is well known that the coefficient of determination cannot be the only indicator used to judge the quality of a model. For this reason, also the Akaike's Information Criterion (AIC) was introduced, since it is particularly indicated for the case of non-nested models (i.e., not dependent)[77]. Because the number of data points N is small with respect to the number of model parameters k, it was

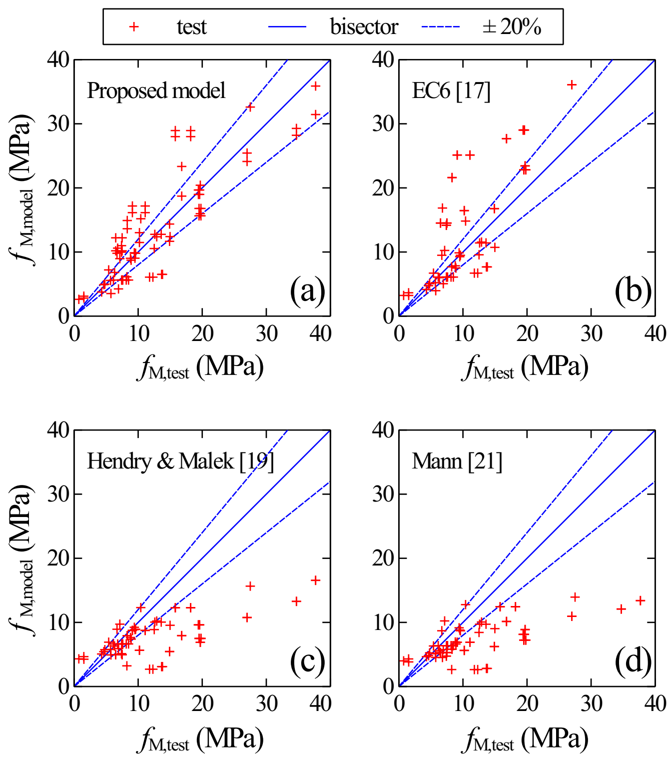

Fig. 7: One-wythe wallettes (all data). Comparison between experimental compressive strengths $f_{M,test}$ and compressive strengths predicted by the calibrated model $f_{M,model}$: (a) Proposed model; (b) EC6 [17]; (c) Hendry & Malek [19]; (d) Mann [21].

preferred to use the corrected Akaike's Information Criterion (AIC_c), defined as:

$$\mathrm{AIC}_c = N \ln \frac{SS}{N} + 2k + \frac{2k(k+1)}{N-k-1} \tag{16}$$

where SS is the sum of squares of the errors X. The coefficient AIC_c can only be computed when $N > 2k$ [77]. Comparing two models, the best one has the lowest AIC_c coefficient.

Also in this case, the proposed model provides better results, particularly when the type of mortar is considered (Tab. 7). It is interesting to notice that, for the proposed model and for EC6, the number of parameters is $k = 2$ because $\alpha + \beta = 1$. For the other two models $k = 3$, therefore the condition $N > 2k$ was not fulfilled in the case of cement-lime and lime mortar, and the coefficient AIC_c was not computed.

Another indicator useful from the engineering point of view is the coefficient a_{20} proposed in [14], which represents the number of points predicted with a relative error $\leq 20\%$ with respect to the total number of points N. Comparing two models, the best one has the a_{20} coefficient closest to one.

If we consider all the data, the models provide similar values of a_{20}, which are close to 0.50. Instead, if the type of mortar is distinguished, the proposed model provides values of a_{20} close to 0.75, which are good and similar to those reached in [14] by means of neural networks.

The study suggests that also the type of mortar should by considered to define the compressive strength of solid-clay-brick wallettes.

Among the models proposed in the literature, the EC6 provides the best results even in the case of lime mortar. This result was not predictable because the model was proposed for general-purpose mortar. Compared to the proposed new models, although the indicators are only slightly worse, the EC6 is more conservative for higher strengths (Fig. 7).

Model	**all**			**cement-lime**			**lime**		
	R^2	a_{20}	AIC_c	R^2	a_{20}	AIC_c	R^2	a_{20}	AIC_c
Proposed	0.73	0.50	42.12	0.77	0.75	17.79	0.72	0.61	19.39
EC6 [17]	0.68	0.50	46.75	0.35	0.63	26.12	0.70	0.50	20.86
Hendry & Malek [19]	0.63	0.53	54.32	0.28	0.38	-	0.63	0.61	27.90
Mann [21]	0.57	0.47	58.42	0.08	0.25	-	0.64	0.61	27.31

Table 7: One-wythe wallettes: comparison of the proposed model to some models published in the literature.

5.2. Stack-bonded prisms

The study proposed for wallettes was repeated for stack-bonded prisms. In particular, Figs. 8, 9 show the relationship between $f_{M,test}$ and $f_{M,model}$ for the cases of $2 < h_M/t_M \leq 3$ and $3 < h_M/t_M \leq 4$ respectively. The same figures show the behavior of the models published for stack-bonded prisms by Lumantarna et al. [20], Kaushik et al. [22], and Gumaste et al. [23].

For the sake of completeness, comparisons with the TMS402/602-16 [78] and AS37000-18 [79] models have been included in in the same figures, even if they are not power models.

The points predicted by the proposed models are well distributed around the bisector line for both slendernesses (Fig. 8a, 9a). On the contrary, the model proposed by Lumantarna [20] fits well the first case with small slenderness (Fig. 8b), but provides unconservative results for the second case (Fig. 9b). This can be explained considering that Lumantarna's model was calibrated for three-bricks-high stack-bonded prisms, which are squat and similar to the first case. The model proposed by Kaushik et al. [22], calibrated for five-bricks-high stack-bonded prisms, provides conservative results in both cases (Figs. 8c, 9c). The same can be said for the model published by Gumaste et al. [23] (Figs. 8d, 9d).

Figs. 8e and 9e show the results for the model proposed in TMS402/602-16 [78]. The ASTM 1314-18 prism test method used for stack-bonded prisms is usually associated with the TMS402/602-16 [78] unit strength method, which provides the specified compressive strength of masonry (in psi) by means of the equation:

$$f_M = A(400 + Bf_b) \tag{17}$$

where f_b is the average compressive strength of clay-masonry units (in psi), $A = 1$ for inspected masonry, $B = 2$ for Type N portland-cement lime mortar, and $B = 0.25$ for type S or M portland-cement lime mortar. The type of mortar is defined with its recipe, which is usually different from those used in the dataset. Moreover, lime mortar is not considered.

Since there is no direct correspondence between mortar strength and type (S, N, or M), $B = 0.2$ for lime mortar and $B = 0.25$ for all other cases were used for the analysis. As can be seen in Figs. 8e and 9e, results overestimate smaller strengths, probably because of the choice of parameter B. Furthermore, the model underestimates higher strengths, as already pointed out in [78].

Finally, the comparisons were carried out with the model proposed in the Australian Standard AS3700-18 [79]:

$$f_M = k_h k_m f_b^{0.5} \tag{18}$$

where f_M and f_b are characteristic strengths, $k_h = \min[1.3, 1.3(19h_m/h_b)^{-0.29}]$ is a joint thickness factor, and k_m is a compressive strength factor which for clay-masonry units and full bedding type it is equal to 1.1, 1.4, and 2.0 for mortar type M2, M3, and M4 respectively. Also in this case it is not easy to find a correspondence between the strength of mortar and its type, therefore it was decided to use $k_m = 1.4$ for lime mortar and $k_m = 2$ for all the other cases. In addition, the characteristic strength provided by Eq. 18 was multiplied by 1.2 to obtain the average strength. For the compressive strength of bricks, the values reported in Tab. A2 were used. For consistency, the correction factor for slendernesses $h_M/t_M < 5$ published by AS3700-18 has been used in place of ASTM 1314-18 to correct the experimental strengths.

Figs. 8f and 9f show the results for AS3700-18 [79] model. Also in this case the model seems to overestimate the lowest strengths and underestimate the highest ones.

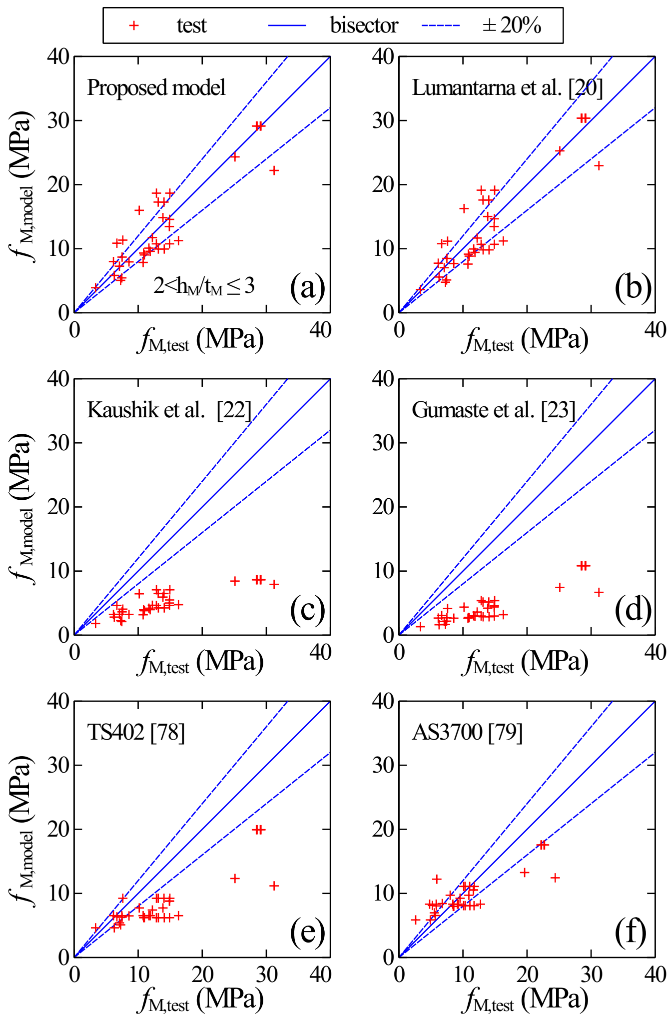

Fig. 8: Stack-bonded prisms with $2 < h_m/t_m \leq 3$. Comparison between experimental compressive strengths $f_{M,test}$ and compressive strengths predicted by the calibrated model $f_{M,model}$: (a) Proposed model ; (b) Lumantarna et al. [20]; (c) Kaushik et al. [22] ; (d) Gumaste et al. [23]; (e) TMS402/602-16 [78]; (f) AS3700-18 [79].

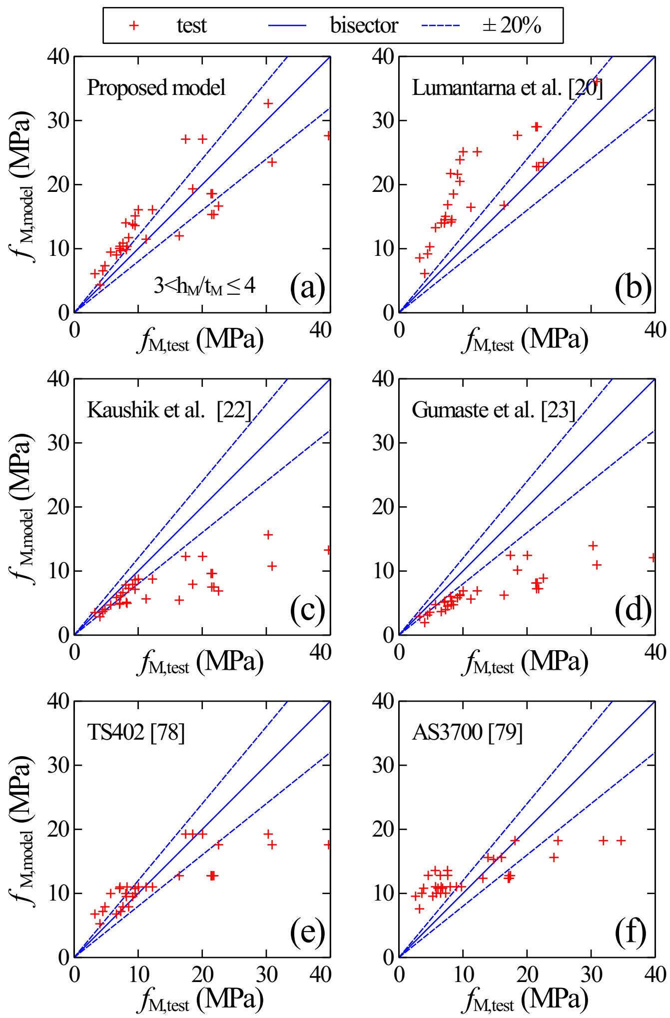

Fig. 9: Stack-bonded prisms with $3 < h_m/t_m \leq 4$. Comparison between experimental compressive strengths $f_{M,test}$ and compressive strengths predicted by the calibrated model $f_{M,model}$: (a) Proposed model ; (b) Lumantarna et al. [20]; (c) Kaushik et al. [22] ; (d) Gumaste et al. [23]; (e) TMS402/602-16 [78]; (f) AS3700-18 [79].

Type	Model	all			cement-lime			lime		
		R^2	a_{20}	AIC_c	R^2	a_{20}	AIC_c	R^2	a_{20}	AIC_c
$2 \leq h_M/t_M < 3$	Proposed	0.82	0.54	86.10	0.57	0.50	62.59	0.24	0.38	24.87
	Lumantarna et al. [20]	0.81	0.46	90.79	0.52	0.36	67.90	0.11	0.38	-
	Kaushik et al. [22]	-1.03	0.00	174.06	-2.25	0.00	109.90	-2.52	0.00	-
	Gumaste et al. [23]	-1.16	0.00	173.64	-3.07	0.00	111.87	-3.53	0.00	39.20
	TMS402/602-16 [78]	0.18	0.14	139.86	-0.91	0.05	95.20	-0.38	0.38	29.71
	AS3700-18 [79]	0.63	0.49	94.58	0.34	0.59	61.07	-0.37	0.5	25.67
$3 \leq h_M/t_M < 4$	Proposed	0.74	0.21	114.33	0.70	0.23	95.03	-	-	-
	Lumantarna et al. [20]	-0.12	0.18	165.49	-0.06	0.23	131.17	-	-	-
	Kaushik et al. [22]	-0.01	0.27	162.03	-0.21	0.23	134.58	-	-	-
	Gumaste et al. [23]	-0.11	0.03	162.71	-0.32	0.00	133.95	-	-	-
	TMS402/602-16 [78]	0.44	0.45	140.42	0.34	0.50	116.09	-	-	-
	AS3700-18 [79]	0.44	0.21	125.79	0.47	0.27	98.99	-	-	-

Table 8: Comparison of the proposed model to the ones published in the literature: Stack-bonded prisms.

The different estimators for the quality of the models are reported in Tab. 8. Considering the coefficient of determination R^2, it is possible to notice that both for the proposed model and for Lumantarna's model, R^2 is about 0.8 if all the specimens are considered and slightly diminishes in the case of cement-lime mortar, also because of the scant number of points.

The models proposed by Kaushik et al. [22], Gumaste et al. [23], and TMS402/602-16 [78] are characterized by poor values of the coefficient of determination R^2, which in some cases are even negative (Tab. 8). In this case, the mean value of the strengths fits better the results than the model. Model AS3700-18 [79], on the other hand, provides slightly better results.

The proposed model presents also the best values of parameters AIC_c and a_{20}, whereas the other models present poor values, similarly to what obtained in [14]. On the contrary, also for these parameters the model AS3700-18 [79] provides acceptable results.

In case of lime mortar, all the models show worse results than those obtained for wallettes.

Results generally confirm that the models proposed in the literature represent well the data used for their calibration but are not able to describe with accuracy the considered dataset, which is characterized by different dimensionless parameters. The AS3700-18 model is a separate case, presumably because it explicitly takes into account more dimensionless parameters (the slenderness of the specimens and the ratio between the thickness of the bed mortar joints and the block). The explicit inclusion of these and other dimensionless parameters is probably the way forward to generalize the power model, allowing a unified approach to compressive strength of masonry.

The proposed regressions are not intended to be, once again, just a calibration of the power equation for the specific case (perhaps they are too many to be adopted in the codes). They rather permit to open a reflection on the adopted procedures and the uncertainties of the results.

6. Conclusions

The power equation is one of the most common phenomenological relationships used in the literature to forecast the compressive strength of masonry, which has been proposed with different coefficients and exponents by many authors. In the present work, the power equation was discussed by means of Dimensional Analysis. Nine dimensionless groups affecting masonry strength were introduced to identify and discuss the field of applicability of the power equation. Then, a dataset of 116 specimens selected from the literature was analyzed considering these dimensionless groups. Subsequently, experimental data were clustered considering the most significant dimensionless groups and used to calibrate new power equations for the different cases. Then, the new models were compared with some power models proposed in the literature. The results indicate that:

- It is proved from the theoretical point of view that the coefficients of the power equation must depend on the geometry of the specimens and on the mechanical properties of the materials. For this reason, the power equations proposed in the literature are specific for the type of specimens (i.e. dimensionless parameters) used for their calibration and direct comparisons among them should be done with great caution.

- A novel representation of the experimental data in the cartesian plane, in terms of dimensionless masonry strength (masonry efficiency) vs. dimensionless mortar strength, permits to observe the importance of specimen type (wallettes or stack-bonded prisms), specimen slenderness, and mortar type (cement, cement-lime, and lime). Furthermore, plots of the collected dataset show that the effect of slenderness is well evident for stack-bonded prism specimens and a suitable correction function should be studied.

- A new calibration of the power equation specific for solid-clay-brick masonry was done considering homogeneous data in terms of dimensionless parameters. Compared to the power models proposed in the literature, the results of fitting are characterized by more consistent estimators. Regressions confirm once again that the power equations proposed in the literature are specific for the type of specimens (i.e. dimensionless parameters) used for their calibration.

- The coefficient of determination R^2 is insufficient to evaluate the quality of a regression. The combination of several estimators, like R^2, Akaike's Information Criterion, and a_{20} seems a good choice for the specific problem, providing more motivated judgments.

The application of the concepts of Dimensional Analysis is new in the field of masonry, where most (if not all) analyses are based on statistical treatment of the measured dimensional variables, with empirical or semi-empirical correlations.

Starting from a broad perspective on masonry compressive strength, the problem was narrowed to the simple case of the power equation. Also in this case the available experiments are by far not enough to perform a thorough analysis in order to leave in place all the variables, hence only the most relevant can be saved. The detailed process of the selection is useful in order to perceive the approximations and the limits of the use of power equations for masonry strength.

The results of the present work are not intended to propose yet another calibration of the power equation but rather to allow a different reading and systematization of the problem, identifying better the context and its limits, and suggesting new developments with the aim of improving the overall approach to the problem.

Acknowledgements

The Author thank Prof. Piero Ganugi and Prof. Marco Riani for the advices on statistics. Furthermore, Prof. Sandro Longo is gratefully acknowledged for the engaging discussions on dimensional analysis. Dr. Erica Lenticchia is gratefully acknowledged for many useful inputs and valuable comments.

This research did not receive any specific grant from funding agencies in the public, commercial, or not-for-profit sectors.

Appendix

N.	ref.	$b_M \times t_M \times h_M$ (mm)	wythes (–)	f_M (MPa)	$b_b \times t_b \times h_b$ (mm)	f_b (MPa)	f'_b (MPa)	h_m (mm)	f_m (MPa)	mortar (–)
1	[36]	$500 \times 250 \times 600$	2	11.00	$250 \times 120 \times 55$	26.90	21.52	10.00	3.20	l
2	[36]	$500 \times 250 \times 600$	2	14.50	$250 \times 120 \times 55$	26.90	21.52	10.00	12.70	c+l
3	[37]	$442 \times 103 \times 385$	1	5.69	$215 \times 103 \times 65$	12.00	10.14	12.00	4.39	l
4	[37]	$442 \times 103 \times 385$	1	6.32	$215 \times 103 \times 65$	12.00	10.14	12.00	7.02	l
5	[37]	$442 \times 103 \times 385$	1	1.53	$215 \times 103 \times 65$	12.00	10.14	12.00	0.89	l
6	[38]	$500 \times 115 \times 370$	1	9.50	$250 \times 115 \times 55$	26.40	22.44	10.00	4.70	l
7	[38]	$500 \times 115 \times 370$	1	9.40	$250 \times 115 \times 55$	26.40	22.44	10.00	5.80	l
8	[38]	$500 \times 115 \times 370$	1	12.90	$250 \times 115 \times 55$	26.40	22.44	10.00	9.80	c+l
9	[39]	$520 \times 110 \times 350$	1	5.40	$- \times 110 \times -$	15.20	12.92	-	5.80	l
10	[39]	$520 \times 110 \times 350$	1	8.80	$- \times 110 \times -$	15.20	12.92	-	9.80	c+l
11	[40]	$280 \times 140 \times 300$	1	8.14	$280 \times 140 \times 55$	19.70	16.74	8.00	2.30	l
12	[40]	$280 \times 140 \times 300$	1	7.42	$280 \times 140 \times 55$	19.70	16.74	8.00	2.30	l
13	[40]	$280 \times 140 \times 300$	1	6.14	$280 \times 140 \times 55$	19.70	16.74	8.00	2.30	l
14	[40]	$280 \times 140 \times 300$	1	7.47	$280 \times 140 \times 55$	19.70	16.74	8.00	2.30	l
15	[40]	$280 \times 140 \times 300$	1	8.50	$280 \times 140 \times 55$	19.70	16.74	8.00	2.30	l
16	[40]	$280 \times 140 \times 300$	1	7.60	$280 \times 140 \times 55$	19.70	16.74	8.00	2.30	l
17	[41]	$660 \times 200 \times 800$	2	1.79	$200 \times 100 \times 70$	7.82	6.81	15.00	1.04	l
18	[42]	$430 \times 100 \times 330$	1	4.64	$200 \times 100 \times 50$	10.00	10.00	-	3.33	c+l
19	[42]	$430 \times 100 \times 330$	1	7.14	$200 \times 100 \times 50$	32.00	32.00	-	2.87	c+l
20	[42]	$430 \times 100 \times 330$	1	10.41	$200 \times 100 \times 50$	32.00	32.00	-	9.84	c+l
21	[43]	$500 \times 120 \times 500$	1	14.98	$250 \times 120 \times 65$	17.40	17.40	13.00	13.85	c
22	[43]	$500 \times 120 \times 500$	1	12.51	$250 \times 120 \times 65$	17.40	17.40	13.00	9.47	c+l
23	[43]	$500 \times 120 \times 500$	1	6.93	$250 \times 120 \times 65$	17.40	17.40	13.00	1.13	l
24	[44]	$380 \times 260 \times 590$	2	6.60	$250 \times 120 \times 50$	15.70	15.70	-	11.10	c+l
25	[44]	$380 \times 260 \times 590$	2	8.30	$250 \times 120 \times 50$	21.20	21.20	-	10.60	c+l
26	[44]	$380 \times 260 \times 590$	2	10.80	$250 \times 120 \times 50$	27.20	27.20	-	10.40	c+l
27	[44]	$380 \times 260 \times 590$	2	5.60	$250 \times 120 \times 50$	16.30	16.30	-	5.80	c+l
28	[44]	$380 \times 260 \times 590$	2	8.00	$250 \times 120 \times 50$	22.20	22.20	-	6.20	c+l
29	[44]	$380 \times 260 \times 590$	2	9.80	$250 \times 120 \times 50$	28.30	28.30	-	5.50	c+l
30	[44]	$380 \times 260 \times 590$	2	9.60	$250 \times 120 \times 50$	28.50	28.50	-	5.80	c+l
31	[23]	$235 \times 115 \times 460$	1	13.60	$235 \times 111 \times 76$	23.00	20.08	12.00	12.21	c+l
32	[23]	$235 \times 115 \times 460$	1	6.70	$235 \times 111 \times 76$	23.00	20.08	12.00	6.60	c
33	[23]	$235 \times 115 \times 460$	1	12.60	$235 \times 111 \times 76$	23.00	20.08	12.00	12.21	c+l
34	[23]	$235 \times 115 \times 460$	1	9.60	$235 \times 111 \times 76$	23.00	20.08	12.00	6.60	c
35	[18]	$700 \times 230 \times 700$	2	5.40	$230 \times - \times 70$	13.10	13.10	10.00	6.10	c

Continued on next page

Table A1 – continued from previous page

N.	ref.	$b_M \times t_M \times h_M$ (mm)	wythes (–)	f_M (MPa)	$b_b \times t_b \times h_b$ (mm)	f_b (MPa)	f'_b (MPa)	h_m (mm)	f_m (MPa)	mortar (–)
36	[45]	440 × 103 × 365	1	8.90	215 × 103 × 65	15.00	12.00	10.00	10.00	l
37	[45]	440 × 103 × 365	1	4.80	215 × 103 × 65	15.00	12.00	10.00	2.70	l
38	[45]	440 × 103 × 365	1	0.74	215 × 103 × 65	15.00	12.00	10.00	0.60	l
39	[45]	440 × 103 × 365	1	1.52	215 × 103 × 65	15.00	12.00	10.00	0.90	l
40	[45]	440 × 103 × 365	1	4.30	215 × 103 × 65	15.00	12.00	10.00	1.40	l
41	[45]	440 × 103 × 365	1	5.75	215 × 103 × 65	15.00	12.00	10.00	1.20	c

Table A1: Database of experimental values: wallettes.

N.	ref.	$b_M \times t_M \times h_M$ (mm)	f_M (MPa)	f'_M (MPa)	$b_b \times t_b \times h_b$ (mm)	f_b (MPa)	f'_b (MPa)	h_m (mm)	f_m (MPa)	mortar (–)
1	[46]	193 × 93 × 465	17.60	21.47	193 × 93 × 53	30.00	23.52	10.00	10.10	c+l
2	[47]	140 × 140 × 300	7.54	7.60	260 × 130 × 55	30.51	25.93	-	2.31	l
3	[48]	250 × 110 × 270	12.50	12.84	250 × 110 × 55	13.80	13.80	10.00	9.20	c+l
4	[48]	250 × 110 × 270	14.50	14.90	250 × 110 × 55	13.80	13.80	10.00	9.20	c+l
5	[48]	250 × 110 × 270	12.80	13.15	250 × 110 × 55	13.80	13.80	10.00	7.00	c+l
6	[48]	250 × 110 × 270	13.70	14.07	250 × 110 × 55	13.80	13.80	10.00	7.00	c+l
7	[40]	240 × 110 × 270	12.51	12.85	240 × 110 × 55	30.50	25.93	10.00	13.10	c+l
8	[40]	240 × 110 × 270	14.55	14.95	240 × 110 × 55	30.50	25.93	10.00	13.10	c+l
9	[40]	240 × 110 × 270	12.78	13.13	240 × 110 × 55	30.50	25.93	10.00	10.00	c+l
10	[40]	240 × 110 × 270	13.66	14.03	240 × 110 × 55	30.50	25.93	10.00	10.00	c+l
11	[49]	191 × 95 × 523	15.56	18.98	191 × 95 × –	34.00	34.00	-	15.70	c
12	[42]	200 × 100 × 330	3.69	4.04	200 × 100 × 50	10.00	10.00	-	3.33	c+l
13	[42]	200 × 100 × 330	6.49	7.10	200 × 100 × 50	32.00	32.00	-	2.87	c+l
14	[42]	200 × 100 × 330	8.70	9.52	200 × 100 × 50	32.00	32.00	-	9.84	c+l
15	[50]	285 × 130 × 280	28.90	29.17	285 × 130 × 50	56.80	68.73	10.00	5.50	c
16	[50]	285 × 130 × 280	28.80	29.07	285 × 130 × 50	56.80	68.73	10.00	5.50	c
17	[50]	285 × 130 × 280	28.20	28.46	285 × 130 × 50	56.80	68.73	10.00	5.50	c
18	[50]	285 × 130 × 280	28.30	28.56	285 × 130 × 50	56.80	68.73	10.00	5.50	c
19	[20]	228 × 112 × 250	3.31	3.36	228 × 112 × 78	8.50	7.50	15.00	1.23	l
20	[20]	228 × 112 × 250	6.98	7.08	228 × 112 × 78	12.00	10.58	15.00	4.54	c+l
21	[20]	228 × 112 × 250	10.70	10.85	228 × 112 × 78	15.70	13.85	15.00	5.53	l
22	[20]	228 × 112 × 250	7.39	7.49	228 × 112 × 78	16.00	14.11	15.00	4.14	c+l
23	[20]	228 × 112 × 250	6.59	6.68	228 × 112 × 78	16.30	14.38	15.00	8.58	l

Continued on next page

Table A2 – continued from previous page

N.	ref.	$b_M \times t_M \times h_M$ (mm)	f_M (MPa)	f'_M (MPa)	$b_b \times t_b \times h_b$ (mm)	f_b (MPa)	f'_b (MPa)	h_m (mm)	f_m (MPa)	mortar (–)
24	[20]	228 × 112 × 250	6.06	6.14	228 × 112 × 78	17.10	15.08	15.00	2.62	l
25	[20]	228 × 112 × 250	12.05	12.22	228 × 112 × 78	21.10	18.61	15.00	5.92	l
26	[20]	228 × 112 × 250	14.70	14.90	228 × 112 × 78	27.30	24.08	15.00	6.65	c+l
27	[20]	228 × 112 × 250	6.19	6.28	228 × 112 × 78	8.50	7.50	15.00	4.95	c+l
28	[20]	228 × 112 × 250	7.17	7.27	228 × 112 × 78	10.60	9.35	15.00	1.75	l
29	[20]	228 × 112 × 250	10.82	10.97	228 × 112 × 78	15.70	13.85	15.00	4.95	c+l
30	[20]	228 × 112 × 250	7.35	7.45	228 × 112 × 78	17.10	15.08	15.00	0.69	l
31	[20]	228 × 112 × 250	10.63	10.78	228 × 112 × 78	17.10	15.08	15.00	2.47	c+l
32	[20]	228 × 112 × 250	11.71	11.87	228 × 112 × 78	17.10	15.08	15.00	4.95	c+l
33	[20]	228 × 112 × 250	11.52	11.68	228 × 112 × 78	17.10	15.08	15.00	5.90	c+l
34	[20]	228 × 112 × 250	16.07	16.29	228 × 112 × 78	17.10	15.08	15.00	8.65	c+l
35	[20]	228 × 112 × 250	14.66	14.86	228 × 112 × 78	27.50	24.25	15.00	4.95	c+l
36	[20]	228 × 112 × 250	30.79	31.22	228 × 112 × 78	38.20	33.69	15.00	12.52	c+l
37	[20]	228 × 112 × 250	24.77	25.12	228 × 112 × 78	43.40	38.28	15.00	12.52	c+l
38	[23]	235 × 115 × 460	6.70	7.70	235 × 111 × 76	23.00	20.08	12.00	6.60	c
39	[51]	240 × 110 × 270	9.90	10.17	240 × 110 × 55	19.90	19.90	10.00	14.72	c+l
40	[51]	240 × 110 × 270	13.50	13.87	240 × 110 × 55	19.90	19.90	10.00	11.39	c+l
41	[52]	230 × 110 × 400	4.00	4.48	230 × 110 × 75	17.70	17.70	10.00	3.10	c
42	[52]	230 × 110 × 400	2.90	3.25	230 × 110 × 75	16.10	16.10	10.00	3.10	c
43	[52]	230 × 110 × 400	5.10	5.72	230 × 110 × 75	28.90	28.90	10.00	3.10	c
44	[52]	230 × 110 × 400	4.30	4.82	230 × 110 × 75	20.60	20.60	10.00	3.10	c
45	[52]	230 × 110 × 400	8.50	9.53	230 × 110 × 75	28.90	28.90	10.00	20.60	c
46	[52]	230 × 110 × 400	7.60	8.52	230 × 110 × 75	20.60	20.60	10.00	20.60	c
47	[52]	230 × 110 × 400	6.50	7.29	230 × 110 × 75	17.70	17.70	10.00	15.20	c+l
48	[52]	230 × 110 × 400	5.90	6.61	230 × 110 × 75	16.10	16.10	10.00	15.20	c+l
49	[52]	230 × 110 × 400	7.20	8.07	230 × 110 × 75	28.90	28.90	10.00	15.20	c+l
50	[52]	230 × 110 × 400	6.80	7.62	230 × 110 × 75	20.60	20.60	10.00	15.20	c+l
51	[6]	194 × 89 × 350	37.70	43.15	194 × 89 × 55	69.80	59.33	7.50	52.60	c+l
52	[6]	194 × 89 × 350	34.70	39.72	194 × 89 × 55	69.80	59.33	7.50	26.40	c+l
53	[6]	194 × 89 × 350	27.00	30.90	194 × 89 × 55	69.80	59.33	7.50	13.70	c+l
54	[6]	194 × 89 × 350	19.70	22.55	194 × 89 × 55	69.80	59.33	7.50	3.40	c+l
55	[53]	250 × 120 × 315	8.24	8.57	250 × 120 × 55	19.76	14.95	10.00	2.62	c
56	[54]	210 × 100 × 340	27.50	30.30	204 × 98 × 50	66.00	66.00	14.00	37.50	l
57	[54]	430 × 100 × 340	18.20	20.06	204 × 98 × 50	66.00	66.00	14.00	17.60	c+l

Continued on next page

Table A2 – continued from previous page

N.	ref.	$b_M \times t_M \times h_M$ (mm)	f_M (MPa)	f'_M (MPa)	$b_b \times t_b \times h_b$ (mm)	f_b (MPa)	f'_b (MPa)	h_m (mm)	f_m (MPa)	mortar (–)
58	[54]	210 × 100 × 340	15.80	17.41	204 × 98 × 50	66.00	66.00	14.00	17.60	c+l
59	[54]	210 × 100 × 340	8.30	9.15	212 × 99 × 51	27.00	27.00	14.00	17.60	c+l
60	[54]	430 × 100 × 340	11.10	12.23	208 × 98 × 50	33.00	33.00	14.00	17.60	c+l
61	[54]	210 × 100 × 340	9.10	10.03	208 × 98 × 50	33.00	33.00	14.00	17.60	c+l
62	[54]	430 × 100 × 340	19.40	21.38	212 × 100 × 53	40.00	40.00	14.00	17.60	c+l
63	[54]	430 × 100 × 340	19.60	21.60	212 × 100 × 53	40.00	40.00	14.00	17.60	c+l
64	[54]	210 × 100 × 340	16.80	18.51	208 × 98 × 50	66.00	66.00	15.00	4.50	c+l
65	[54]	210 × 100 × 340	7.40	8.15	212 × 99 × 51	27.00	27.00	14.00	4.50	c+l
66	[54]	210 × 100 × 340	10.20	11.24	208 × 98 × 50	33.00	33.00	14.00	4.50	c+l
67	[54]	430 × 100 × 340	19.80	21.82	212 × 100 × 53	40.00	40.00	12.50	8.10	c+l
68	[54]	430 × 100 × 340	19.50	21.49	212 × 100 × 53	40.00	40.00	12.50	8.10	c+l
69	[54]	430 × 100 × 340	7.50	8.26	208 × 98 × 50	33.00	33.00	14.00	3.00	c+l
70	[54]	210 × 100 × 340	6.50	7.16	208 × 98 × 50	33.00	33.00	14.00	3.00	c+l
71	[54]	430 × 100 × 340	14.90	16.42	212 × 100 × 53	40.00	40.00	14.00	3.00	c+l
72	[55]	290 × 140 × 273	12.30	12.13	290 × 140 × 50	21.30	17.04	10.00	1.23	l
73	[55]	290 × 140 × 265	11.78	11.43	290 × 140 × 50	21.30	17.04	10.00	1.23	l
74	[55]	290 × 140 × 265	13.80	13.39	290 × 140 × 50	21.30	17.04	10.00	1.90	l
75	[55]	290 × 140 × 268	13.66	13.33	290 × 140 × 50	21.30	17.04	10.00	1.90	l

Table A2: Database of experimental values: stack-bonded prisms.

References

[1] Engesser F. Über weitgespannte wölbbrücken. Zeitschrift für Architekturs und Ingenieurwesen 1907;53:403–40.

[2] Circolare n. 7/19 . Istruzioni per l'applicazione dell'aggiornamento delle norme tecniche per le costruzioni di cui al D.M. 17 gennaio 2018, G.U. n. 35/2019. Ministero delle Infrastrutture e dei Trasporti; (in Italian); 2019.

[3] Dymiotis C, Gutlederer BM. Allowing for uncertainties in the modelling of masonry compressive strength. Constr Build Mater 2002;16(8):443–52.

[4] Garzón-Roca J, Marco CO, Adam JM. Compressive strength of masonry made of clay bricks and cement mortar: Estimation based on neural networks and fuzzy logic. Eng Struct 2013;48:21–7.

[5] Hendry AW. Structural masonry. Palgrave Macmillan; 2nd ed.; 1998.

[6] McNary WS, Abrams DP. Mechanics of masonry in compression. J Struct Eng-ASCE 1985;111(4):857–70.

[7] Haller P, Sinclair DA. The technological properties of brick masonry in high buildings. Canada NRC Technical Translation Tt; National Research Council of Canada, Division of Building Research; 1959.

[8] Biolzi L. Evaluation of compressive strength of masonry walls by limit analysis. J Struct Eng-ASCE 1988;114(10):2179–89.

[9] Uday Vyas C, Venkatarama Reddy B. Prediction of solid block masonry prism compressive strength using FE model. Mater Struct 2010;43(5):719–35.

[10] Lourenço PB, Pina-Henriques J. Validation of analytical and continuum numerical methods for estimating the compressive strength of masonry. Comput Struct 2006;84(29):1977–89.

[11] Drougkas A, Roca P, Molins C. Numerical prediction of the behavior, strength and elasticity of masonry in compression. Eng Struct 2015;90:15–28.

[12] Zahra T, Dhanasekar M. Prediction of masonry compressive behaviour using a damage mechanics inspired modelling method. Constr Build Mater 2016;109:128–38.

[13] Thamboo J, Dhanasekar M. Nonlinear finite element modelling of high bond thin-layer mortared concrete masonry. International Journal of Masonry Research and Innovation 2016;1(1):5–26.

[14] Asteris PG, Argyropoulos I, Cavaleri L, Rodrigues H, Varum H, Thomas J, et al. Masonry compressive strength prediction using artificial neural networks. In: Moropoulou A, Korres M, Georgopoulos A, Spyrakos C, Mouzakis C, editors. Proc. of the 1st Int. Conf. TMM_CH, Transdisciplinary Multispectral Modelling and Cooperation for the Preservation of Cultural Heritage, Athens, Greece, October 10-13, 2018. Springer; 2019, p. 10–3.

[15] Ferretti D, Coïsson E, Ugolotti D, Lenticchia E. Use of EC6-like equations to estimate the compressive strength of masonry made of solid clay bricks and lime mortar. In: Modena C, da Porto F, Valluzzi M, editors. Proc. of the 16th Int. Brick and Block Masonry Conference, Padova, Italy, 26-30 June 2016. Taylor & Francis Group, London; 2016, p. 1561–70.

[16] Liberatore D, Marotta A, Sorrentino L. Estimation of clay-brick unreinforced masonry compressive strength based on mortar and unit mechanical parameters. In: Lourenço PB, Haseltine B, Vasconcelos G, editors. Proc. of 9th International Conference of Masonry, Guimarães, Portugal, 07-09 July 2014. 2014, p. 1–12.

[17] Eurocode 6 . EN 1996-1-1:2005: Design of masonry structures - Part 1-1: General rules for reinforced and unreinforced masonry structures. 2005.

[18] Malek MH. Compressive strength of brickwork masonry with special reference to concentrated load. Ph.D. thesis; Dept. of Civil Engrg. and Civil Sciences, University of Edimburgh; 1987.

[19] Hendry AW, Malek MH. Characteristic compressive strength of brickwork walls from collected test results. Masonry Int 1986;7:15–24.

[20] Lumantarna R, Biggs DT, Ingham JM. Uniaxial compressive strength and stiffness of field extracted and laboratory constructed masonry prisms. J Mater Civil Eng 2014;26(4):567–75.

[21] Mann W. Statistical evaluation of tests on masonry by potential functions. In: Proc. of the 6th International Brick Masonry Conference, ROme, Italy, 16-19 May 1982. (in German): ANDIL; 1982, p. 77–83.

[22] Kaushik HB, Rai DC, Jain SK. Stress-strain characteristics of clay brick masonry under uniaxial compression. J Mater Civil Eng 2007;19(9):728–39.

[23] Gumaste KS, Rao KSN, Reddy BVV, Jagadish KS. Strength and elasticity of brick masonry prisms and wallettes under compression. Mater Struct 2007;40(2):241–53.

[24] Dayaratnam P. Brick and reinforced brick structures. South Asia Books; 1987.

[25] Barenblatt GI. Scaling, self-similarity, and intermediate asymptotics: dimensional analysis and intermediate asymptotics (Cambridge Texts in Applied Mathematics). Cambridge University Press; 1996. ISBN 978-0521435222.

[26] Szirtes T. Applied dimensional analysis and modeling. Butterworth-Heinemann; 2007. ISBN 0123706203.

[27] Longo S. Analisi dimensionale e modellistica fisica. Springer Milan (in Italian); 2011. ISBN 8847018714.

[28] Thaickavil NN, Thomas J. Behaviour and strength assessment of masonry prisms. Case Studies in Construction Materials 2018;8:23–38. doi: 10.1016/j.cscm.2017.12.007.

[29] Grimm CT. Strength and related properties of brick masonry. Journal of the Structural Division 1975;101(1):217–32.

[30] fib Federation Internationale du Beton . fib Model Code for Concrete Structures 2010. Ernst W. + Sohn Verlag; 2013. ISBN 3433030618.

[31] Caporale A, Parisi F, Asprone D, Luciano R, Prota A. Comparative micromechanical assessment of adobe and clay brick masonry assemblages based on experimental data sets. Compos Struct 2015;120:208–20. doi: 10.1016/j.compstruct.2014.09.046.

[32] Sonin AA. A generalization of the Π-theorem and dimensional analysis. Proc of the National Academy of Sciences 2004;101(23):8525–6. doi: 10.1073/pnas.0402931101.

[33] Zucchini A, Lourenço PB. Mechanics of masonry in compression: Results from a homogenisation approach. Comput Struct 2007;85(3-4):193–204.

[34] Augenti N, Parisi F, Acconcia E. Mada: online experimental database for mechanical modelling of existing masonry assemblages. In: Proc. of the 15th World Conference on Earthquake Engineering, Lisbon, Portugal, 24-28 Sept 2012. SPES; 2012, p. 24–8.

[35] Sarangapani G, Venkatarama Reddy BV, Jagadish KS. Brick-mortar bond and masonry compressive strength. J Mater Civil Eng 2005;17(2):229–37.

[36] Binda L, Fontana A, Frigerio G. Mechanical behaviour of brick masonries derived from unit and mortar characteristics. In: Courcy JWD, editor. Proc. of the 8th Int. Brick and Block Masonry Conference, 19-21 Sept 1988, Trinity College, Dublin; vol. 1. Elsevier Applied Science; 1988, p. 205–16.

[37] Costigan A, Pavía S. Compressive, flexural and bond strength of brick/lime mortar masonry. In: Mazzolani F, editor. Proc. of International Conference on Protection of Historical Buildings PROHITECH09, Rome, Italy, 21-24 June 2009. CRC Press; 2009, p. 1609–15.

[38] Mattone R, Pasero G, Pavano M, Pistone G, Roccati R. Prove sperimentali su campioni di varie dimensioni volte alla determinazione delle caratteristiche meccaniche delle vecchie murature. In: Proc. of the 6th Int. Brick Masonry Conference, Rome 16-19 May 1982, (in Italian). ANDIL; 1982, p. 198–209.

[39] Pistone G, Roccati R. Mechanical characteristics of masonry rebuilt with ancient bricks and fresh mortars. In: Proc. of the 9th Int. Brick & Block Masonry Conference, Berlin, Germany, 13-16 Oct 1991. Berlin: Deutsche Gesellschaft für Mauerwerksbau; 1991, p. 1473–80.

[40] Brencich A, de Felice G. Brickwork under eccentric compression: Experimental results and macroscopic models. Constr Build Mater 2009;23(5):1935–46.

[41] Ignatakis C, Stylianides K. Mechanical characteristics of virgin and strengthened old brick masonry- experimental research. Masonry Int 2004;17(1):9–17.

[42] Vermeltfoort AT. Mechanical properties under compression of masonry and its components. In: Proc. of the 6th Canadian Masonry Symposium. 1992, p. 657–62.

[43] Bosiljkov V. Micro vs. macro reinforcement of brickwork masonry. Mater Struct 2006;39(2):235–45.

[44] Zago F, Riva G. Proprietà fisico-meccaniche dei mattoni e comportamento della muratura del centro storico di Venezia. Parte seconda: la muratura. Scuola Tipografica Emiliana Artigianelli, Venice, (in Italian) 1982;45:1–23.

[45] Costigan A, Pavía S, Kinnane O. An experimental evaluation of prediction models for the mechanical behavior of unreinforced lime-mortar masonry under compression. Journal of Building Engineering 2015;4:283–94.

[46] Maurenbrecher AHP. Effect of test procedures on compressive strength of masonry prisms. In: Proc. of the 2nd Canadian Masonry Symposium. Ottawa; 1980, p. 119–32.

[47] de Felice G. Experimental investigation on historic brickwork subjected to eccentric axial loads. In: Proc. of the 5th Int. Conf. on Structural Analysis of Historical Constructions SAHC06. Macmillan India Ltd New Delhi,, India; 2006, p. 809–16.

[48] Brencich A, Corradi C, Gambarotta L. Eccentrically loaded brickwork: Theoretical and experimental results. Eng Struct 2008;30(12):3629–43.

[49] Ewing BD, Kowalsky MJ. Compressive behavior of unconfined and confined clay brick masonry. J Struct Eng-ASCE 2004;130(4):650–61.

[50] Oliveira DV, Lourenço PB, Roca P. Cyclic behaviour of stone and brick masonry under uniaxial compressive loading. Mater Struct 2006;39(2):247–57.

[51] Brencich A, Gambarotta L. Mechanical response of solid clay brickwork under eccentric loading. Part I: Unreinforced masonry. Mater Struct 2005;38(2):257–66.

[52] Kaushik HB, Durgesh CR, Sudhir KJ. Uniaxial compressive stress-strain model for clay brick masonry. Current Science 2007;92(4):497–501.

[53] Panizza M, Garbin E, Valluzzi MR, Modena C. Experimental investigation on bond of FRP/SRP applied to masonry prisms. In: Proc. of 6th Int. Conference on FRP Composites in Civil Engineering (CICE 2012), 13-15 June 2012, Rome, Italy. 2012, p. 1–8.

[54] Vermeltfoort A, Martens D, Van Zijl G. Brick-mortar interface effects on masonry under compression. Can J Civil Eng 2007;34(11):1475–85.

[55] Drougkas A, Roca P, Molins C. Compressive strength and elasticity of pure lime mortar masonry. Mater Struct 2016;49(3):983–99.

[56] Thamboo JA, Dhanasekar M. Correlation between the performance of solid masonry prisms and wallettes under compression. Journal of Building Engineering 2019;22:429–38.

[57] EN 1052-1:1998 . Methods of test for masonry: Determination of compressive strength. 1998.

[58] ASTM1314-14 . Standard Test Method for Compressive Strength of Masonry Prisms - C1314-14. West Conshohocken, PA.: ASTM International; 2014.

[59] Binda L, Mirabella Roberti G, Tiraboschi C. Problemi di misura dei parametri meccanici della muratura e dei suoi componenti. In: Proc. of La meccanica delle murature tra teoria e progetto, 18-20 Sept. 1996, Messina (Italy) (In Italian). 1996, p. 45–56.

[60] EN 772-1:2000 . Methods of test for masonry units Part 1: determination of compressive strength. 2011.

[61] Zhou Q, Wang F, Zhu F. Estimation of compressive strength of hollow concrete masonry prisms using artificial neural networks and adaptive neuro-fuzzy inference systems. Constr Build Mater 2016;125:417–26. doi:http://dx.doi.org/10.1016/j.conbuildmat.2016.08.064.

[62] Sarhat SR, Sherwood EG. The prediction of compressive strength of ungrouted hollow concrete block masonry. Constr Build Mat 2014;58:111–21. doi:http://dx.doi.org/10.1016/j.conbuildmat.2014.01.025.

[63] Lumantarna R. Material characterisation of New Zealand's clay brick unreinforced masonry buildings. Ph.D. thesis; The University of Auckland Department of Civil and Environmental Engineering; New Zealand; 2012.

[64] Antonelli C. Risultati di esperimenti eseguiti sulla resistenza alla compressione di alcuni pilastrini in muratura. L'Ingegneria Civile e le Arti Industriali, (in Italian) 1885;11(1):1–5.

[65] Krefeld WJ. The effect of shape of specimens on the apparent compressive strength of brick masonry. ASTM Proceedings 1938;38(1):363–9.

[66] Noland JL, Hanada KT, Feng CC. The effect of slenderness and end coefficients on the strength of clay unit prisms. In: Proc. of the 1st North American Masonry Conference. 1978, p. 14–1–14–27.

[67] Kingsley GR, Noland JL, Shuller MP. The effect of slenderness and end restraint on the behavior of masonry prisms: a literature review. TMS Journal 1992;10:31–47.

[68] Hamid AA, Chukwunenye AO. Compression behavior of concrete masonry prisms. Journal of Structural Engineering 1986;112(3):605–13.

[69] Fahmy EH, Ghoneim TGM. Behaviour of concrete block masonry prisms under axial compression. Canadian Journal of Civil Engineering 1995;22(5):898–915.

[70] Korany Y, Glanville J. Comparing masonry compressive strength in various codes. Concrete international 2005;27(7):35–9.

[71] Hassanli R, ElGawady MA, Mills JE. Effect of dimensions on the compressive strength of concrete masonry prisms. Advances in Civil Engineering Materials 2015;4(1).

[72] Mathworks . Statistics and Machine Learning Toolbox; 2016. URL `http://www.mathworks.com/help/stats/index.html`.

[73] Riani M, Perrotta D, Torti F. Fsda: A matlab toolbox for robust analysis and interactive data exploration. Chemometrics and Intelligent Laboratory Systems 2012;116:17–32.

[74] Carino NJ. Statistical methods to evaluate in-place test results. ACI Special Publication 1993;141:39–64.

[75] ACI 228.1 R-03 . In-place methods to estimate concrete strength. ACI Committee 228; 2003.

[76] Mandel J. Fitting straight lines when both variables are subject to error. J Qual Technol 1984;16(1):1–14.

[77] Anderson D, Burnham K. Model selection and multi-model inference. NY: Springer-Verlag; 2nd ed.; 2004.

[78] TMS 402/602-16 . Building Code Requirements and Specifications for Masonry Structures. 2016.

[79] AS3800:18 . Masonry Structures. Australian Standard; 2018.

Notes